Title
Automated, Label-free Analysis of Rare, Large Cells from Blood

Author
Go, Derek Eno

Publication Date
2014

Peer reviewed|Thesis/dissertation

UNIVERSITY OF CALIFORNIA

Los Angeles

Automated, Label-free Analysis of Rare, Large Cells from Blood

A thesis submitted in partial satisfaction

of the requirements for the degree Master of Science

in Bioengineering

by

Derek Eno Go

2014

ABSTRACT OF THE THESIS

Automated, Label-free Analysis of Rare, Large Cells from Blood

by

Derek Eno Go

Master of Science in Bioengineering

University of California, Los Angeles, 2014

Professor Dino Di Carlo, Chair

Cancer cells found in circulation, termed circulating tumor cells (CTCs), are believed to disseminate from tumors and form secondary metastatic sites. These malignant cells may provide a crucial source to characterize and monitor malignancy but they exist among billions of blood cells and are extremely rare (1-500 CTCs/mL blood). Developing isolation and analysis methods rely on antibodies targeted towards CTC surface markers but their heterogeneous expression indicates the need for alternative methods of analysis that correlate more with malignancy.

We use a recently introduced microfluidic device that can selectively isolate and concentrate large (> 15 μm) cells from blood. The label-free and high-purity isolation achieved enables passive analysis of the isolated cells, which can give a quick readout about the suitability for further downstream assays. Correlating label-free characteristics of CTCs to disease state may provide more accurate clinical information for cancer diagnosis, treatment monitoring, and personalized therapy identification.

The thesis of Derek Eno Go is approved.

Benjamin M. Wu

Daniel T. Kamei

Dino Di Carlo, Committee Chair

University of California, Los Angeles

2014

Dedication

Mom, Dad, and Martin

Table of Contents

Acknowledgements

Chapter I

This chapter is an adaptation and expansion of the introduction section of Chapter II.

Chapter II

Label-free Isolation of Large Circulating Cells from Whole Blood has been reprinted with adaptations with permission from (E. Sollier, D. E. Go, J. Che, D. R. Gossett, S. O'Byrne, W. M. Weaver, N. Kummer, M. Rettig, J. Goldman, N. Nickols, S. McCloskey, R. P. Kulkarni, and D. D. Carlo, "Size-selective collection of circulating tumor cells using Vortex technology," *Lab. Chip*, vol. 14, no. 1, pp. 63–77, Nov. 2013.) Copyright (2013) Royal Society of Chemistry. Professor Dino Di Carlo is the principal investigator of this work. This work was supported by funding from a Coulter Translational Research Award (Wallace H. Coulter Foundation), the Office of Naval Research Young Investigator Program (Grant #N000141210847), and a sponsored research grant from NetScientific.

Chapter III

Label-free Analysis of All Isolated Cells is a version of work in preparation for publication by Derek E. Go, James Che, Manjima Dhar, Edward Pao, Victor Yu, Edward Garon, Jonathan Goldman, Rajan Kulkarni, Elodie Sollier, and Dino Di Carlo. Professor Dino Di Carlo is the principal investigator of this work. This work was supported by funding from a sponsored research grant from NetScientific.

Chapter IV

Cytological and Cytogenetic Analysis of Circulating Tumor Cells is a version of work in preparation for publication by Derek E. Go, Sean O'Byrne, Jianyu Rao, Nagesh Rao, Edward Garon, Jonathan Goldman, Rajan Kulkarni, Elodie Sollier, and Dino Di Carlo. Professor Dino Di

Carlo is the principal investigator of this work. This work was supported by funding from a sponsored research grant from NetScientific.

Additional Acknowledgements:

Thanks to the countless friends I've made through this experience that have taught, encouraged, and inspired me:

Jaideep S. Dudani, Jonathan Lin, Dr. Henry Tse, Dr. Daniel R. Gossett, Sean O'Byrne, Professor Aram Chung, Ivan Pushkarsky, Dr. Elodie Sollier, Dr. Albert J. Mach, Dr. Peter Tseng, Dr. Westbrook Weaver, Dr. Mahdokht Masaeli, Dr. Hamed Amini, Dr. Oladunni Adeyiga, Dr. Anja Kunze, Dr. Donghyuk Kim, Coleman Murray, Keegan Owsley, Jerry Wu, James Che, Harsha Kittur, Janay Kong, Manjima Dhar, Edward Pao, Dr. Rajan Kulkarni, Dr. Nagesh Rao, and all clinical collaborators in UCLA Pathology and Radiation Oncology.

I am especially thankful to Professor Dino Di Carlo for his mentorship, support, and exceptional kindness.

Lastly, I am extremely grateful to my friends and especially my family for their constant love and support.

I. Introduction

The dissemination of a primary tumor to secondary sites through a process known as metastasis is responsible for 90% of all cancer-associated mortalities[1]. In many of these cases, patients were diagnosed and treated after their cancers had already spread, which diminishes current treatment from having its highest efficacy[2]. Thus, detecting metastases, especially at early stages, provides crucial information to physicians for disease staging, monitoring, and management to maximize patient survival[3][4]. Secondary tumors are traditionally detected via imaging techniques such as positron emission tomography (PET) and computed tomography (CT) but they have limited utility for early detection and treatment monitoring. Imaging resolution limits physicians from detecting metastases until they are millimeters in size, at which point patient life expectancy has already diminished[5][6]. Physicians must also image all probable metastatic sites but cannot do so in a frequent fashion to monitor treatment efficacy, given the hazards of repeated exposure.

There has been interest in recent years to study circulating tumor cells (CTCs), which are believed to enter the circulation from a primary tumor and initiate cancerous growths at secondary sites (Figure 1)[7][8]. Although the cellular mechanism is still under investigation, numerous studies have demonstrated a correlation between high frequency of CTCs in the blood and advanced disease progression[9][10]. This indicates the potential for physicians to use these malignant cells to gain clinically valuable insight towards staging primary tumors and invasiveness as well as monitoring response to treatment and recurrence. Because these cells circulate in the bloodstream, they are also easily accessible through a simple blood draw or “liquid biopsy” that can provide a real-time prognostic indicator and possibly a marker for early detection[11][12][13].

CTCs may also provide a valuable source for cellular and molecular analysis, especially for personalized therapies[11]. An emerging trend in cancer therapy is the use of pharmacological agents that target specific molecular pathways affected by common genetic lesions[14].

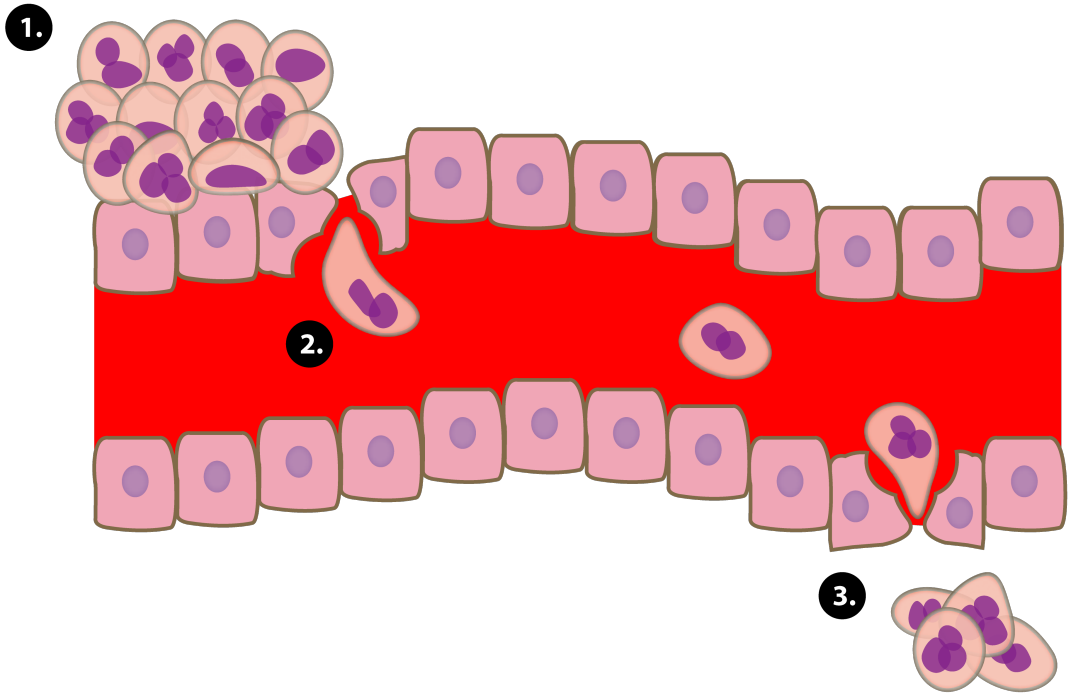

Figure 1: Proposed cellular mechanism of cancer metastasis. Cells from an initial tumor (Step 1) slough off into circulation (Step 2) until they initiate formation of a secondary tumor (Step 3).

These drugs are only effective in patients with those specific molecular lesions and can also diminish in efficacy due to the emergence of resistance. As a result, drug treatments must be individualized following molecular analysis of the tumor by detecting the presence of particular mutations or drug-resistant mutations[14][15][16]. In some cases, the primary tumor can be biopsied and cancer cells analyzed, but the primary tumor is typically already surgically removed or is otherwise inaccessible, and CTCs constitute an ideal alternative.

Analyzing CTCs also has potential to impact cancer research[17][11]. It has been hypothesized that an epithelial-to-mesenchymal transition (EMT) is responsible for activating an invasive phenotype in cells of the primary tumor[9]. Though this is currently under study, performing downstream molecular characterization on isolated cells would enable genomic and proteomic information to be extracted and analyzed to elicit molecular signatures of this

activation. These pathways could then be targeted by developing new drugs to potentially inhibit or prevent metastasis.

However, emerging technologies must overcome technical challenges to reliably isolate CTCs and realize this potential. These malignant cells are extremely rare, even among patients with advanced metastatic disease. Additionally, these cells exist in a high background of contaminating blood components. For instance, one milliliter of blood contains five billion red blood cells (RBCs), 100 million white blood cells (WBCs), and possibly only 1-500 CTCs[18]. This necessitates a highly sensitive and specific isolation method.

Developing techniques have achieved isolation by targeting CTC-specific biomarkers[11][19][20][21]. The current gold standard and only FDA-approved device for CTC enumeration is CellSearch by Veridex. This system requires target cells to be immunomagnetically separated from blood using EpCAM-conjugated magnetic microparticles (EpCAM is presumed to be present on carcinomas, which arise from epithelial origin)[22][23]. Cells captured are then fixed and labeled with fluorescent antibodies to increase specificity of the assay. Other affinity-based technologies are being developed which operate on the principles of affinity chromatography, such that cells with EpCAM coated surfaces preferentially adhere to the high device surface area. Anti-EpCAM is immobilized on the chip surfaces and blood is flowed through the device at a controlled rate to maximize specific binding[12][24][25].

However, these binding affinity approaches are limited by throughput, releasing captured cells, and heterogeneous EpCAM expression. The time necessary per run is at least several hours, and production may be costly due to the need for expensive antibodies and surface chemistry quality control[12][24]. Furthermore, the cells cannot easily be removed from the microchannel or coated surfaces once attached, which may limit further analysis for molecular signatures or downstream culture[26]. Most importantly, affinity-based technologies do not capture all types of CTCs, as capture is based upon the expression of EpCAM. However, cancer experiences intra/inter-tumor heterogeneity that manifests in molecular differences

between tumors of different patients and even within cells of the same tumor[27]. EpCAM expression is no exception, and thus CTCs with little to no EpCAM expression may not be isolated[28][29]. Specific antibodies to other surface markers can be employed instead; however, prior knowledge of the surface expression of a protein may be unavailable and will likely vary significantly between patients and different cancer types.

This has motivated researchers to achieve label-free isolation to meet this challenge. For instance, Tan et al. proposed and commercialized an appealing technology (Captor system, from Abnova) for the label-free isolation and enumeration of CTCs in a series of crescent-shaped microwells, but this approach was capable of analyzing < 2mL of blood with additional steps for CTC release afterwards[30]. Toner et al. recently introduced a platform named CTC-iChip, combining magnetic-affinity-based capture for positive or negative depletion - with both deterministic lateral displacement and inertial focusing[31]. This new approach improved greatly upon previous performance in terms of throughput, efficiency, integrity of cells collected and applicability to non-epithelial cancers and larger sample volumes. Additionally, Hou et al. introduced the use of spiral channels and Dean vortices for CTC enrichment, and interestingly provided viable CTCs in suspension independently of marker expression as well. The throughput for continuous CTC collection is high compared to other techniques (3mL/h)[32].

The low purity (0.1% and 10%, respectively) of these approaches necessitates the use of immunostaining assays to discern captured white blood cells from potential CTCs. Standard CTC detection assays post-isolation model the CellSearch method, where CTCs are defined as positive for cytokeratin (epithelial cell marker) and negative for CD45 (leukocyte marker). However, cytokeratin expression also suffers from intra/inter-tumor heterogeneity. Additionally, false-positive cytokeratin expression in neutrophils has been reported and encountered in our work as well[33]. This demonstrates a need to not only achieve label-free isolation but also to perform other types of analysis in addition to improve accuracy.

These isolation technologies have utilized cytology and cytogenetics, which involves analyzing cell morphologies and molecular signatures, to improve their accuracy of analysis[31][34]. These techniques, however, especially with affinity-based isolation methods, are unable to easily release cells after binding and isolation. This complicates facile integration with automated and well-established clinical laboratory equipment and has required developing unique protocols to adapt to their technologies. In addition, the low purity isolation achieved presents a barrier to clinical translation, which makes it difficult to analyze cells of interest with a high background. Here, we utilize a recently introduced microfluidic device that can selectively concentrate larger cells from blood for label-free isolation and analysis[35][36][37]. Isolated cells in suspension can be released on-demand from the device and easily interfaced with traditional label-based analysis in addition to standard clinical analysis for more thorough and accurate characterization (Figure 2).

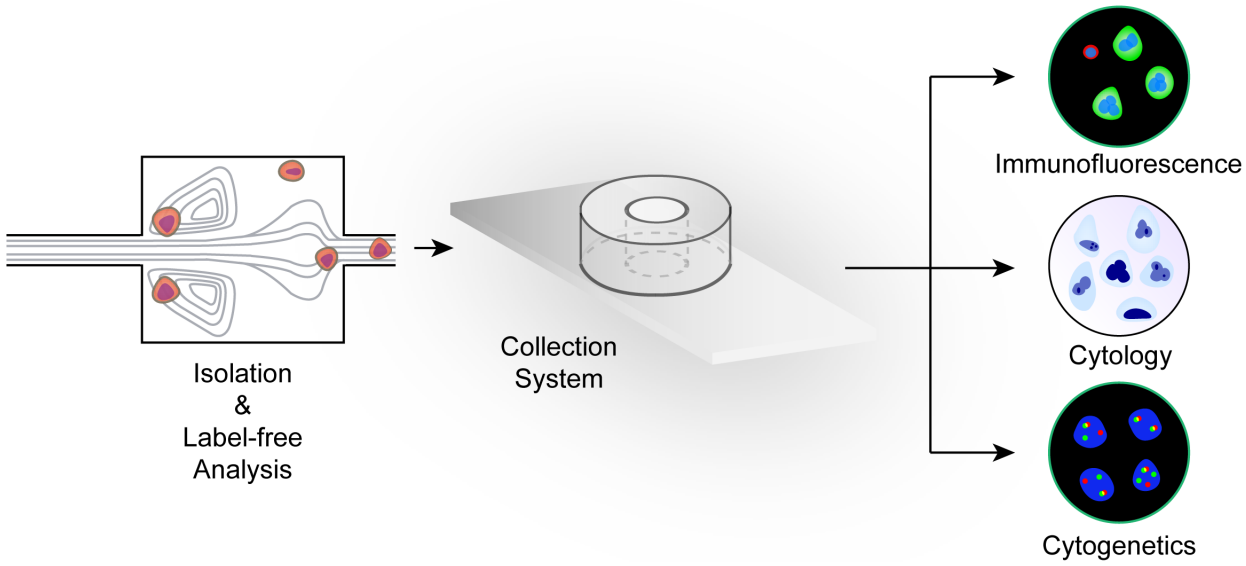

Figure 2: Improving accuracy of CTC analysis. Process flow of label-free isolation followed by multiple modes of analysis. First, label-free analysis can be performed on-chip while cells are gathered in a collection system. This enables seamless integration with standard clinical protocols such as immunocytochemistry, cytology, and cytogenetics. In conjunction, these analysis procedures improve the accuracy of CTC analysis.

II. Label-free Isolation of Large Circulating Cells from Whole Blood

A miniaturized microfluidic system has previously been developed that integrates the high-throughput operations of enrichment and concentration of a standard centrifuge, with the isolation of larger cells from complex fluids. By using micro-scale vortices and inertial focusing, larger cells of interest can be selectively isolated and concentrated while smaller cells are flushed out of the device.

As first experimentally visualized by Segre and Silberberg in 1961 and more recently engineered by Di Carlo and others, inertial focusing uses the effects of fluid inertia in shaped microchannels to align microparticles and cells at high flow rates (Figure 3A)[38][39][40]. When randomly dispersed particles flow through a rectangular channel with a particle Reynolds number, Re_P, of order 1 or greater (Figure 3B), they are subjected to two counteracting inertial lift forces: (i) a shear-gradient lift force F_{LS}, scaling as $F_{LS} = f_L \rho U_m^2 a^3 / W_C$ that directs particles toward the channel walls, and (ii) a wall effect lift force F_{LW}, scaling as $F_{LW} = f_L \rho U_m^2 a^6 / W_C^4$, that is due to the presence of the wall and repels the particles toward the channel centerline (Figure 3C)[41]. $Re_P = Re(a/W_C)^2$ where a/W_C is the ratio of particle diameter to the channel's smaller width, and Re is channel Reynolds number $Re = \rho U_m D / \mu$. Here D is the hydraulic diameter of the channel, U_m is the maximum velocity of the fluid with density ρ and dynamic viscosity μ, while f_L is the dimensionless lift coefficient. In square or rectangular channels, the combination of these forces leads to the migration of particles to two to four dynamic equilibrium positions (X_{eq}) located between the channel centerline and the wall[42].

The second part of this technology makes use of multiple expansion-contraction reservoirs placed in series and parallel, which generate multiple vortices when flow of a sample occurs at high Q and Re (Figure 3D). An inertial boundary layer separation accounts for these predictable laminar vortices (i.e. Moffatt corner eddy flow) that occur at sudden expansions in microscale channels[43]. Particle motion in the vicinity of these recirculating flow regions has

been further investigated and widely used for cell separation, while Hur et al. first demonstrated that these vortices could be used for size-based cancer cell concentration[35].

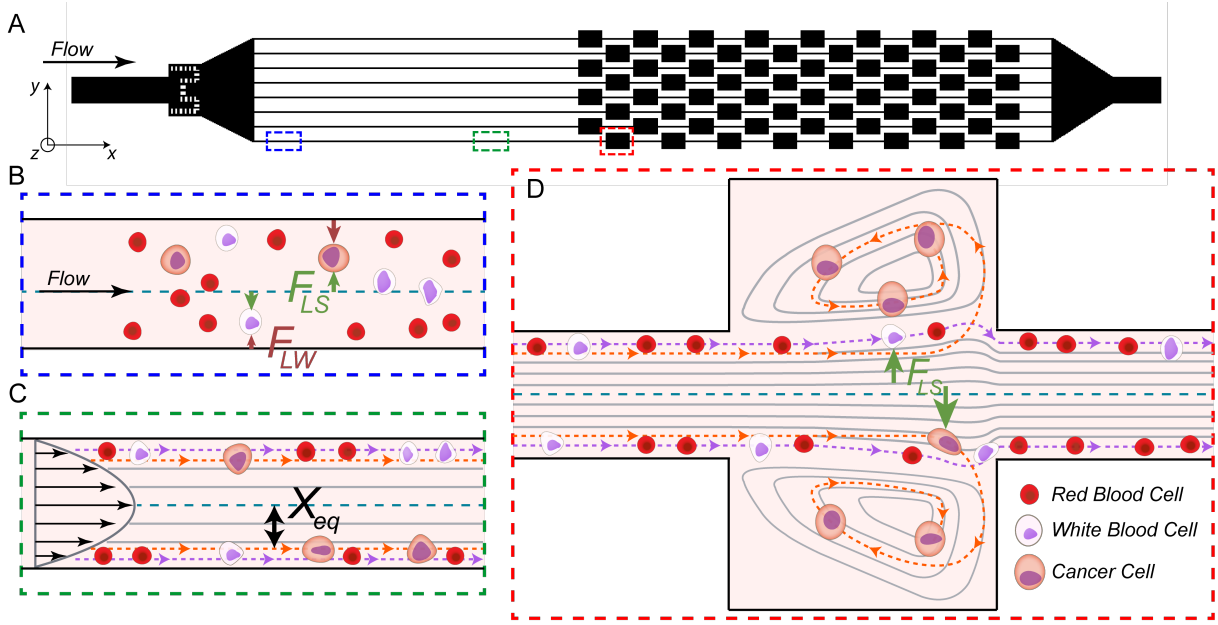

Figure 3: Vortex chip design and principle. (A) The Vortex chip used for cell trapping consists of 8 channels (W_C=40 μm, H=80-85 μm, L_C=4 mm) in parallel with 8 reservoirs (W_R=480 μm, L_R=720 μm) per channel, and each channel is 1 mm apart. (B) At the channel inlet, cells are randomly distributed and experience two opposite lift forces, the wall effect F_{LW} and the shear-gradient lift force F_{LS}. (C) As a result, particles migrate to dynamic lateral equilibrium positions, X_{eq}, depending on the channel cross section. (D) Upon entrance into the reservoir, the wall effect is reduced. Larger cells (violet dashed line) still experience a large F_{LS}, and are pushed away from the channel center through the separatrix and into the vortices, where they are stably trapped. Smaller cells (red dashed line) do not experience enough F_{LS} to cross the separatrix and remain in the main flow.

The use of straight inertial focusing channels upstream from the vortex reservoirs allows cells to dynamically focus to equilibrium positions in proximity to the channel walls, aiding in entry into vortices downstream[39]. As discussed above when the cells enter an expanding

reservoir, the wall effect becomes negligible but cells are still exposed to F_{LS}, which is directed toward the vortex center. Since the shear-gradient lift force scales with a^3, larger particles experience a larger lateral lift force, which directs them towards the vortex core after crossing fluid streamlines and passing through the separatrix (i.e. the boundary between the main flow and the secondary vortex patterns). Cells larger than a defined size cut-off can be selectively isolated in reservoirs and continuously orbit stably in the micro-vortices generated, while smaller particles remain in the main stream. After a wash step that removes any remaining small particles, large particles may then be released in a small, concentrated liquid volume (~300 μL) by simply lowering the flow rate. The microvortices generated in this geometry are different from the vortices generated in the streamwise direction, such as Dean vortices created in curved channels or due to asymmetrically structured microchannels[44].

To demonstrate the ability to isolate CTCs from tumors with variable EpCAM expression levels, we modeled a patient blood sample by injecting cultured cancer cells at clinically relevant concentrations (~200 cells/mL) into diluted blood. We then compared the recovery and purity for 5 different cancer cell lines from different cancer origins and with different levels of EpCAM expression (Figure 4A, 4B): breast MCF7 and ovarian OVCAR5 carcinomas models high expression (around 500,000 antigens/cell), prostate PC3 carcinoma models medium expression (50,000 antigens/cell), lung A549 carcinoma models low expression, and finally melanoma M395, which are not of epithelial origin. Melanoma M395 and breast MCF7 have similar sizes (17.72 and 17.69 μm) and are both captured well, with >20% efficiency, where capture efficiency (%) is defined by $\frac{Target\ Cells\ Captured}{Target\ Cells\ Introduced} \times 100\%$. Ovarian OVCAR5 are smaller (16.78 μm) but still yield an efficiency of 15.9%. Lung A549 have a size (15.90 μm) closest to the 15 μm size cut-off, which may explain the lower efficiency of 7.7%. Finally, despite their larger size (18.21 μm), prostate PC3 are extracted at efficiencies below 9%. Interestingly, the purity of cells enriched is higher than 75%, where purity (%) is defined as $\frac{Target\ Cells\ Captured}{Total\ Cells\ Captured} \times 100\%$ which is

vital for downstream applications. Thus, the vortex chip is not restricted to epithelial cells only and does not need costly antibodies or antibody cocktails but requires that cancer cells possess a larger diameter than normal blood cells.

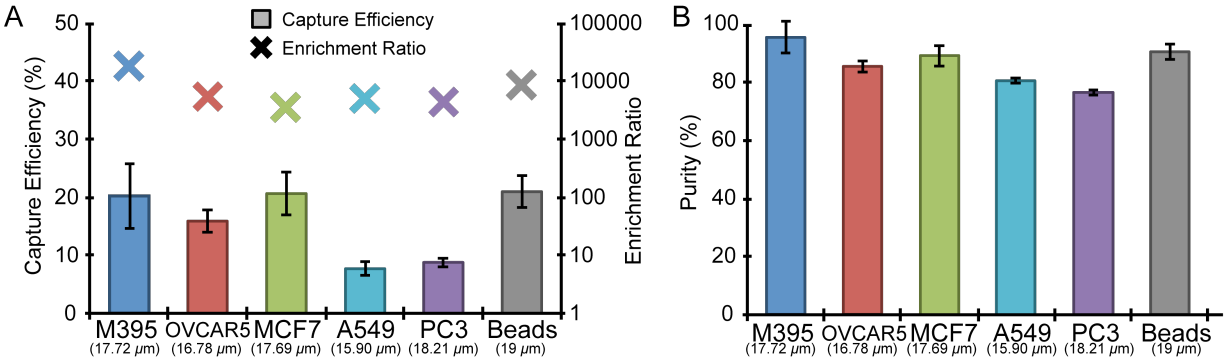

Figure 4: Collection of viable cancer cells from blood. (A) Capture Efficiency and (B) Purity for various cancer cell lines (M395 melanoma, OVCAR5 ovarian carcinoma, MCF7 breast carcinoma, A549 lung carcinoma, PC3 prostate adenocarcinoma, and 19 μm polystyrene beads) independently of EpCAM expression. *Enrichment Ratio* is defined as the purity of the eluent collected divided by the purity of the native sample: $\frac{Target\ cells\ in\ eluent}{Nucleated\ cells\ in\ eluent} \Big/ \frac{Target\ cells\ in\ eluent}{Nucleated\ cells\ in\ eluent}$.

Materials and Methods

Microfluidic device design and fabrication

Microfluidic devices were fabricated using common polydimethylsiloxane (PDMS) replica molding processes[44]. Briefly, standard lithographic techniques were used to produce a mold from a silicon master wafer spin-coated with KMPR 1050 (Microchem). PDMS chips were produced from this mold using Sylgard 184 Elastomer Kit (Dow Corning Corporation) and a cross-linker to polymer ratio of 1:10. To enclose the channels, PDMS and glass were both activated by O_2 plasma (Technics Micro-RIE series 800, 500 mTorr, 80 Watts, 30 sec) before being bonded together.

The Vortex chip used for cell trapping is composed of 64 reservoirs, with 8 paths in parallel and 8 reservoirs per path (Figure 3A). Each path is comprised of a single straight high-aspect ratio channel (W_C=40 µm, H=80-85 µm, L_C=4 mm) followed by 8 reservoirs (W_R=480 µm, L_R=720 µm) located every 1 mm downstream. Filters located at the inlet prevent channel clogging by bead or cell aggregates or debris present in blood samples.

Particles, cells and blood

15 and 19 µm polystyrene particles (CV 1%, 3000 particles/mL ± 10% and CV≤16%, 10% w/w, respectively) were purchased from Thermo Scientific and diluted in PBS at a defined spiking concentration. All cell lines were cultured in the growth media suggested by American Type Culture Collection (ATCC) and incubated at 37 °C in 5% CO_2 to 30-40% confluency. MCF7 (breast carcinoma, ATCC) were cultured in medium containing DMEM supplemented with 10% FBS and 1% penicillin/streptomycin (Invitrogen). OVCAR-5 (ovarian carcinoma), M395 (melanoma), PC-3 (prostate adenocarcinoma) cell lines were cultured in RPMI 1640 medium supplemented with 10% FBS and 1% penicillin/streptomycin (Invitrogen). A549 (lung carcinoma) cell lines were cultured with F12-K medium, 10% FBS and 1% penicillin/streptomycin (Invitrogen). Blood specimens were collected from healthy volunteers under IRB-approved protocol (UCLA-IRB#11-001120), into EDTA tubes (BD Vacutainer) by trained physicians, stored at room temperature, and processed within 24 hours.

Our experiments required spiking known amounts of beads/cancer cells in PBS or blood samples. Particle number was determined by transferring a 100-µL volume of particle solution into a 96-well plate. The well was then imaged using fluorescence microscopy to count the number of particles. For low spiking ratios, three wells were imaged and averaged to give the cell spiking concentration. 100 µL of particle solution was spiked into each PBS/blood sample for the experiments described below.

Particle injection, trapping, release and observation

For experiments using flow-rate control: a simple two-inlet / two-syringe pump system enables rapid solution exchange within the device. One inlet was connected to a syringe containing the sample (beads or cells, spiked in PBS or diluted blood) while the second inlet was connected to a syringe containing PBS as a washing buffer. All solutions were injected into the devices through PEEK tubing (Upchurch Scientific Product No. 1569) using syringe pumps (Harvard Apparatus PHD 2000) and plastic syringes for flow rates ranging from 2 to 12 mL/min. The sample was continuously agitated during the injection to maintain a uniform concentration throughout the experiment.

Before cell/particle injection, the vortices are developed and stabilized in each reservoir by flowing PBS at 4 mL/min (Priming Step). The cell suspension is then injected in the device to trap particles/cells in the reservoirs (Capture Step). In parallel, maintaining the pressure inside the buffer reservoir prevents back-flow of the sample into the buffer solution. After sample injection, PBS buffer is introduced into the device at 4 mL/min to wash out untrapped blood cells (Washing Step). Finally, cells trapped in the vortices are released on-demand by lowering the buffer flow rate, escape from reservoirs, and are collected in a 96-well plate (Release Step).

During each experiment, on-chip particle/cell injection, capture and release were recorded using Phantom v7.3 high-speed camera and Phantom Camera Control and Software (Vision Research Inc.). Live observations allow us to check for the presence of debris or bubbles, which could perturb the trapping experiments. Each well of collected particles was imaged using a Photometrics CoolSNAP HQ2 CCD camera mounted on a Nikon Eclipse Ti microscope, with an ASI motorized stage operated with Nikon NIS-Elements AR 3.2 software. Images were automatically captured for up to four configurations: brightfield, DAPI, FITC, and TRITC filter sets. *Capture Efficiency* is defined as the number of cells/particles collected off-chip over the number of particles injected (i.e. spiked at the inlet). Capture reproducibility is estimated using the average of 3 independent experiments, i.e. using 3 different microfluidic devices.

Cancer cell isolation from spiked blood samples

For spiking experiments, cells were prepared with trypsin and incubated in media at room temperature on a shaker plate for 20 minutes to allow for ample recovery from trypsin treatment. Cells were spiked in blood and injected immediately. A Coulter counter (Beckman Coulter Z2, Cell and Particle Counter) was used to measure average cell size before each injection. Blood was diluted with PBS 10Xand spiked with a known number of cells. Typically, there were about 200-700 cells spiked in 1 mL of whole human blood diluted with 9 mL PBS for 10X dilution.

Isolated cells were collected into a 96-well plate for fixation, permeabilization, and immunolabeling: cells in suspension were treated with 4% v/v paraformaldehyde for 15 min, permeabilized with 0.4% v/v Triton X-100 (Sigma-Aldrich) for 7 min, and incubated with CK-PE (BD), DAPI (Invitrogen) and CD45-FITC (Invitrogen) in 2% w/v BSA for leukocyte, epithelial, and nuclear stains, with PBS washing between each step. After staining, the cells were imaged and enumerated to quantify capture efficiency, enrichment, and purity. *Capture Efficiency* for cancer cells is defined as the number of cancer cells captured in the 96-well-plate (CK+, DAPI+ and CD45-) over the number of cells spiked into diluted human blood. *Capture Purity* is defined as the ratio of cancer cells captured to the total number of captured cells (all nucleated cells DAPI+). *Enrichment Ratio* is defined as the purity in the outlet divided by the purity in the inlet, i.e. *ER*=(cancer cells/nucleated cells in outlet) / (cancer cells/nucleated cells in inlet).

III. Label-free Analysis of All Isolated Cells

Traditional techniques employ antibody-based labeling protocols after isolation to discern CTCs from a low purity isolation[12][25][45]. CTCs are typically defined as positive for cytokeratin, a marker for cells of epithelial origin, and negative for CD-45, a leukocyte-specific marker. Leukocytes are defined as negative for cytokeratin and positive for CD-45. However, the expression of cytokeratin in cancer, as with EpCAM, suffers from heterogeneous expression. It has also been reported and encountered in our own studies that cytokeratin can give false-positive signals with neutrophils (Figure 5)[33]. Furthermore, studies proposing an EMT mechanism in malignant cells show a loss of epithelial markers, including EpCAM and cytokeratin[9]. Thus, a potentially crucial population of circulating cells may remain undetected with epithelial markers as a biomarker of CTCs.

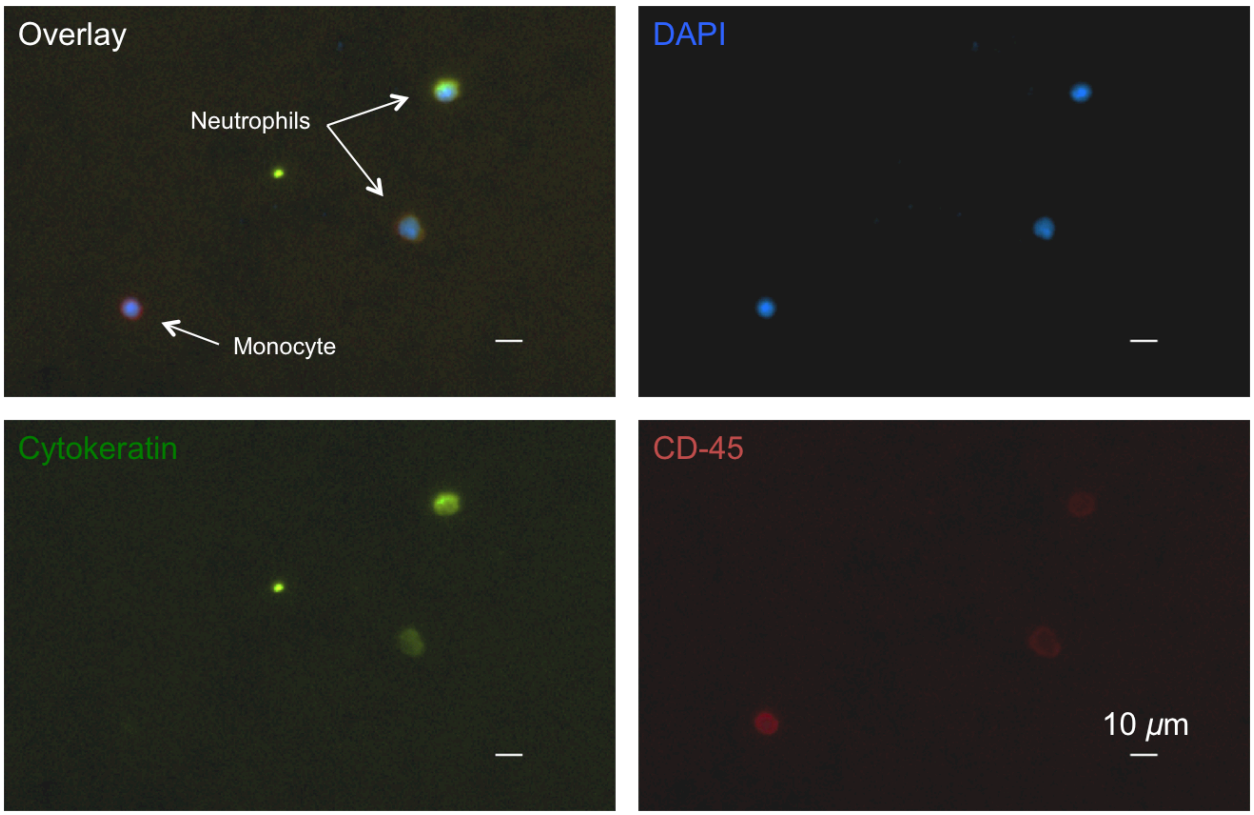

Figure 5: False-positive cytokeratin signals in neutrophils. As reported by others, cytokeratin yields false-positive signals in neutrophils and indicate that these cells are positive for

cytokeratin, an epithelial marker, and CD45, a leukocyte marker. Neutrophils should theoretically give negative signals for cytokeratin because they are not from epithelial origin and positive signals for CD45.

The highly pure isolation achieved from the Vortex chip (> 75%, Figure 4) can potentially enable label-free enumeration and analysis of all isolated cells where the small subpopulation of white blood cells can potentially be treated as a systematic offset. If this low background of contaminating cells is relatively constant across healthy and cancer patient samples, this could eliminate the need for label-based detection assays and their associated limitations. However, the small contaminating population of other isolated cells must be analyzed to see if its contributions to the overall cell population are discernable. To further understand this, cells isolated from clinical samples were compared in terms of their immunofluorescent classifications compared to all isolated cells. First looking at a size distribution of cells isolated from a Stage IV (highly developed, differentiated, metastasizing tumor) non-small cell lung cancer (NSCLC) patient sample, a wide size distribution of cells that stained positive for cytokeratin and a smaller subpopulation of cells positive for CD45 were isolated (Figure 6). When looking at the size distribution of all DAPI positive cells isolated, which corresponds to all nucleated cells, a similar trend can be seen, where there are a few small cells (~ 10 μm) that correspond to white blood cells and a population of larger cells (>10 μm) that corresponds to CTCs.

To compare CTC counts between label-based and label-free analysis following isolation with the Vortex chip, enumeration from immunofluorescence detection was compared to enumeration of all nucleated cells. For a sample set of 46 clinical samples (27 NSCLC, 7 breast, 12 healthy controls), the label-based method indicated a background level of cytokeratin positive cells in healthy samples (Mean = 5.22 cells/mL, Median = 4.59 cells/mL, Figure 7). This increased in comparison to healthy, as expected, in Stage IV NSCLC patients (Mean = 15.22

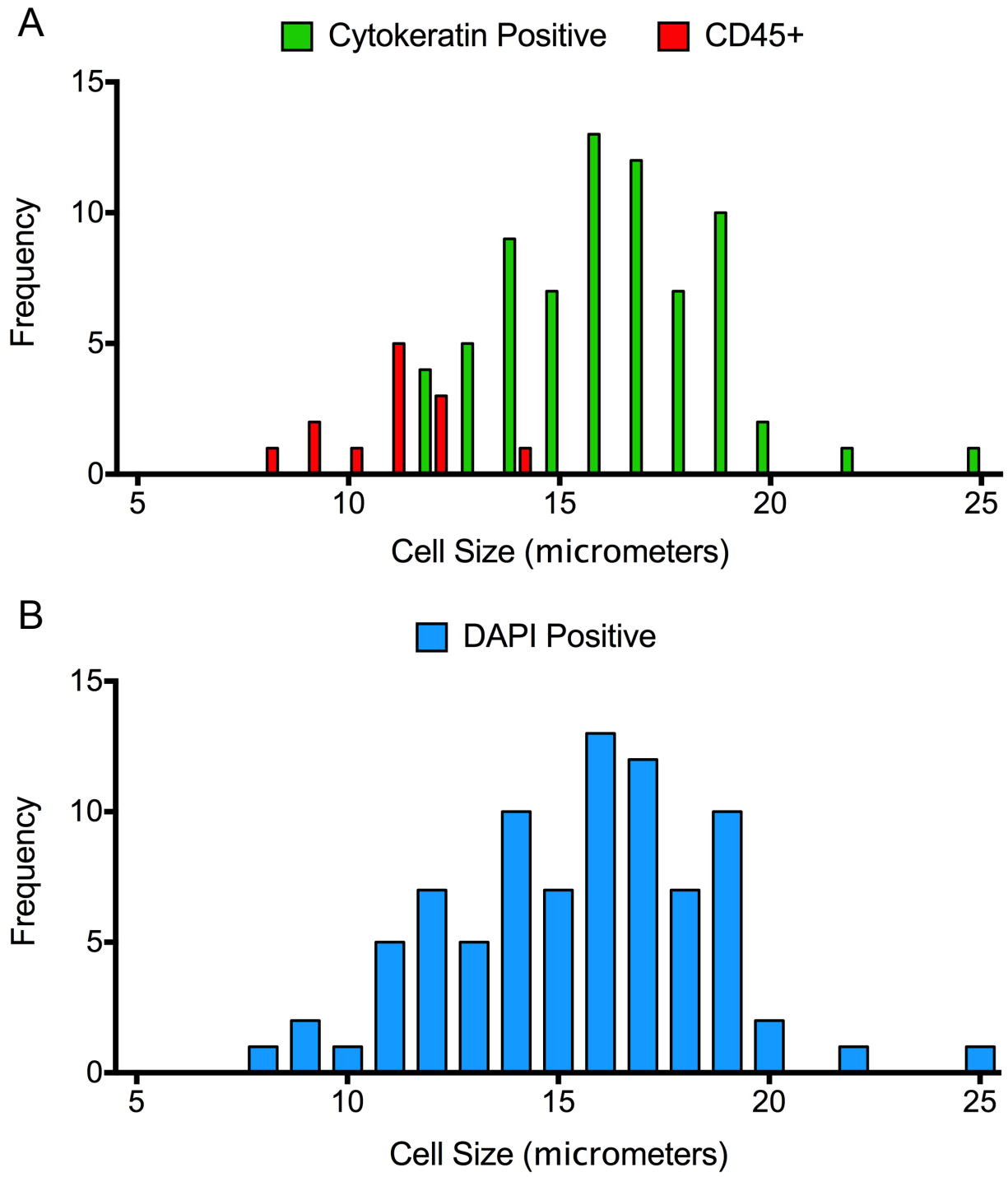

Figure 6: Comparing size distributions of immunofluorescence assays and all cells isolated from the Vortex chip. (a) Size measurements of an immunostained cell population (non-small cell lung cancer, NSCLC, patient sample) isolated with the Vortex Chip demonstrate a highly pure population of large circulating tumor cells (defined as cytokeratin positive). (b) High purity

enables accurate analysis of the entire cell population (defined as DAPI positive) without the need for complex, manual, and costly staining. The data from the entire isolated cell population varies only slightly from the data retrieved through immunofluorescence analysis, which motivates label-free analyses methods.

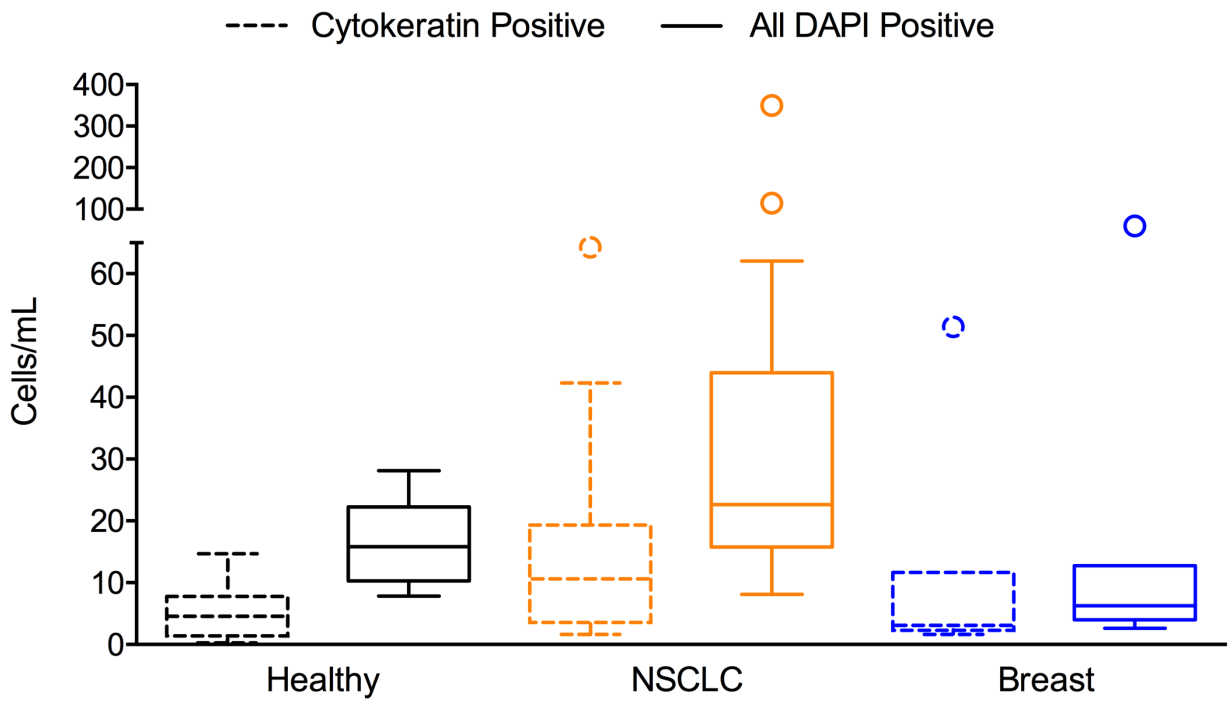

Figure 7: Comparing CTC counts of immunofluorescence assays and all cells isolated from the Vortex chip. Immunofluorescence analysis of cells isolated from non-small cell lung cancer (NSCLC) and breast cancer patient samples reveal an increase of cytokeratin positive cells compared to healthy samples, which can also be seen with the inclusion of all other captured cells.

cells/mL, Median = 10.63 cells/mL) but interestingly decreased in Stage IV breast cancer patients (Mean = 3.07 cells/mL, Median = 11.13 cells/mL). We hypothesize that this could be attributed to the presence of smaller metastatic cells in breast cancer or statistical variation in a relatively smaller sample size in which patients are at all different stages of treatment. Comparing to counts of all nucleated cells, we see that these trends are recapitulated. There is

an increase in the background signal of cells isolated from healthy patients (Mean = 16.23 cells/mL, Median = 15.82 cells/mL) as well as an increase in the NSCLC patients (Mean = 42.76 cells/mL, Median = 22.64 cells/mL) and breast patients (Mean = 18.16 cells/mL, Median = 6.25 cells/mL) which reconstitutes the same trend shown as with the immunofluorescence assay. This demonstrates the feasibility to move towards an assay in which all isolated cells from a cancer patient sample are enumerated and compared to all isolated cells from a healthy patient.

To further motivate label-free analysis following high purity isolation from the Vortex chip, a receiver operating characteristic (ROC) analysis was performed on the same NSCLC and healthy samples to compare CTC counts from immunofluorescence analysis to all nucleated cells (Figure 8). A defined cutoff at > 11.81 cytokeratin positive cells/mL gives a sensitivity of 48.15% and a specificity of 91.67%, whereas a cutoff of > 26.49 isolated cells/mL gives a sensitivity of 44.44% and a specificity of 91.67%. Interestingly, the area under the curve (AUC) increases when analyzing all cells (0.7346 vs. 0.7608), indicating that the small background of contaminating cells does not significantly affect the accuracy of the assay. The sensitivity of the assay is low for both methods, however, which may be caused by the wide distribution of patients with varying treatment at the time of sample collection. Furthermore, we envision this not as a diagnostic assay alone but rather as a quick readout to determine suitability for further cytological and cytogenetic analysis, both of which will increase sensitivity.

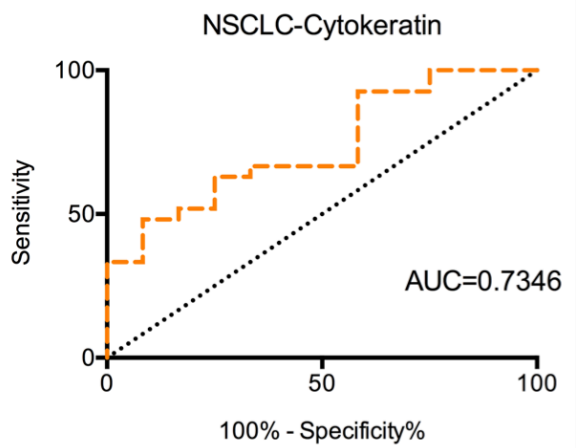

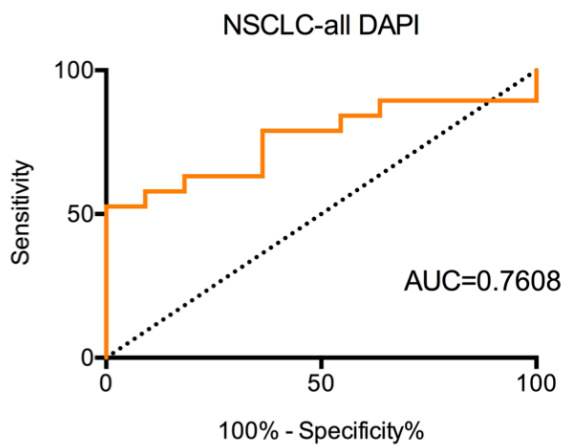

Figure 8: Receiver operating characteristic analysis of enumeration from immunofluorescence of NSCLC compared to healthy samples yields an area under the curve of 0.7346. The analysis of all isolated cells from NSCLC and healthy samples yields a slightly higher area under the curve of 0.7608, demonstrating further motivation towards a label-free assay. These ROC curves also enable the detection of abnormal levels of circulating cells that indicate the need for further analysis (cytological, molecular).

The capabilities of the Vortex chip allow facile integration with a passive and automated system to perform label-free analysis. Because the device achieves highly pure isolation and can release cells on-demand in a small concentrated volume, a high-speed camera can be interfaced to image a static 'imaging area' located at the device outlet (Figure 9). By reducing the pressure supplied to achieve optimal fluid flow for cell isolation, the captured cells are released from the vortices and cells pass through this imaging area at around 0.2 m/s. The acquired video is then analyzed through an automated script to extract a total cell count and cell physical measurements. Using a MATLAB custom-built code, the size distribution of captured cells are extracted from the image sequences.

Using a background subtraction method, the intensity values of an empty frame are subtracted from each ensuing image of the video, which eliminates the background image and yields traces of incident particles in the frames in which they appear (Figure 10). Each individual image is also magnified three times to improve the accuracy of the measurements, which in essence helps achieve sub-pixel resolution. The images are converted to binary and the particle traces are then filled with morphological closing (erosion followed by dilation) and measured for their diameter and circularity. Data from the detected particles/cells is then plotted in histogram form to visualize their size distribution. This can be compared to data collected from healthy patients, which can help to reveal abnormalities that may be correlated to disease state and the need for additional modes of analysis.

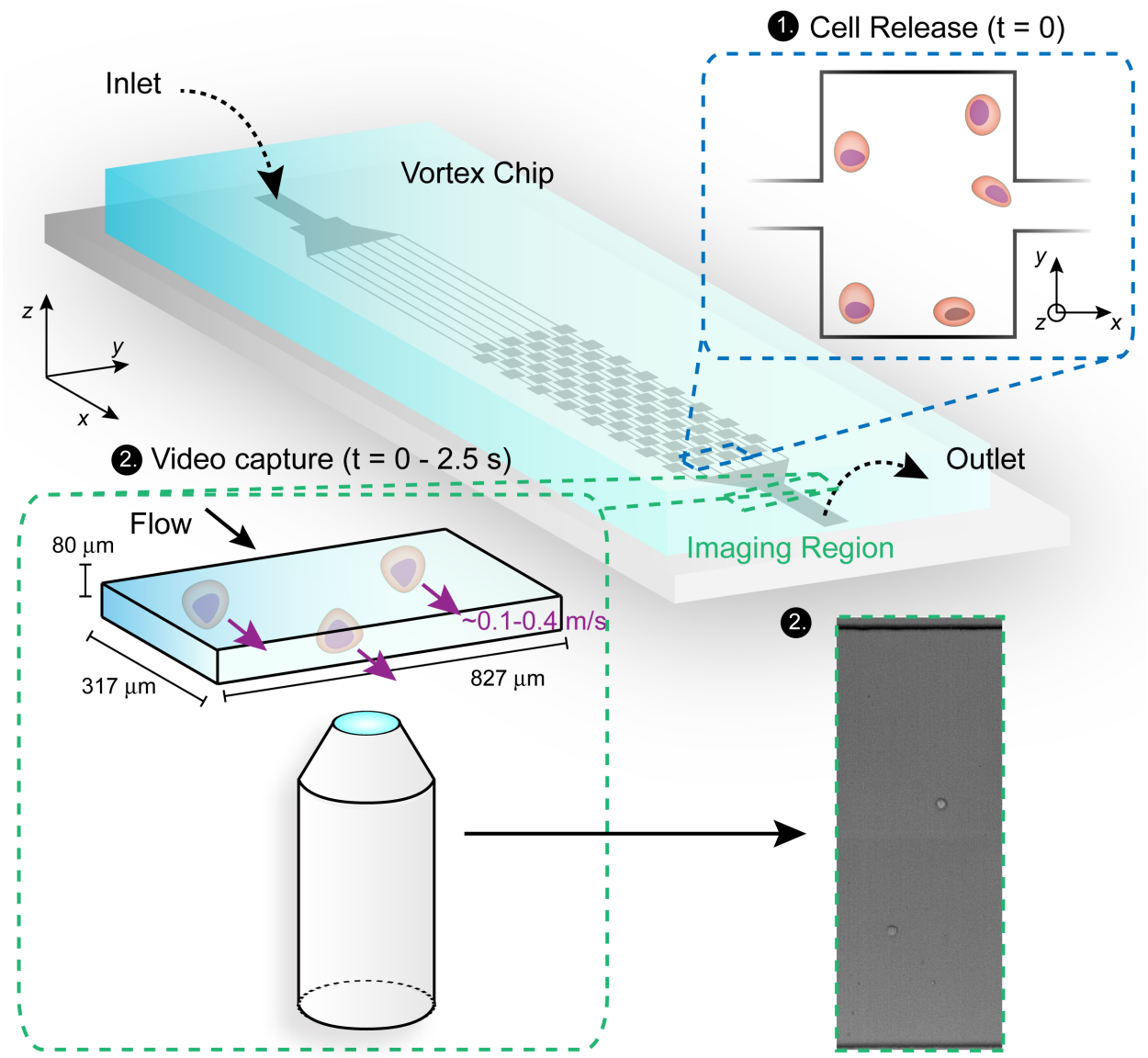

Figure 9: Label-free Analysis with the Vortex Chip. Isolated cells are released from the Vortex Chip (Step 1, t = 0 sec) and are imaged as they pass through the imaging region (Step 2). Cells traverse this region at speeds of 0.1-0.4 m/s, which depends on time after release. The captured high-speed video, which is taken at a suitable frame rate to either capture one or multiple measurements per cell, can then be analyzed with the custom automated MATLAB script.

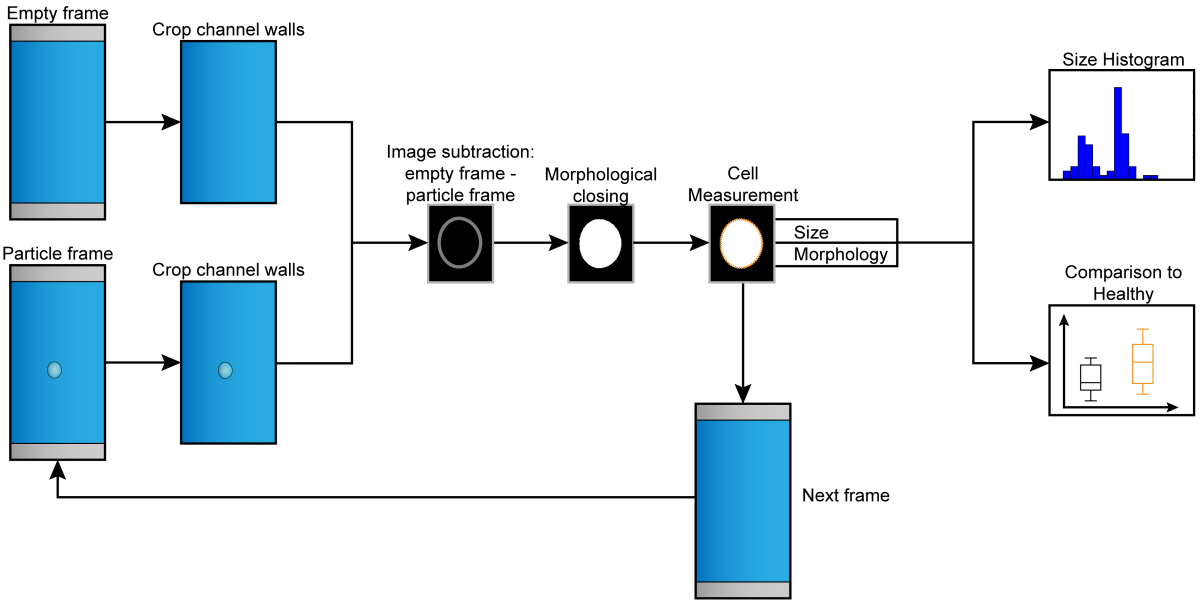

Figure 10: Automated Cell Measurement Script. A MATLAB custom-built code reads through images of a captured video and returns cell count, size, and morphology measurements. First, the channel walls of the device are cropped from every frame of the captured video to avoid any errors during cell detection and measurement. The script then reads an image without any particles (empty frame) and subtracts the corresponding intensity values from every subsequent frame. Thus, in the frames in which cells appear, cell traces are obtained. The resulting images are then resized 3x to increase the accuracy of measurements to submicron resolution. After, the images are converted to binary and the cell traces are filled with morphological closing (erosion followed by dilation) so that they can be measured for physical properties. The results can be plotted as a size histogram and compared to data from healthy patients, which can reveal abnormalities that correlate to disease state and the need for further modes of analysis.

This simplistic method enables full automation at low-cost, label-free, and is a passive measurement technique. Given the nature of the video required for analysis, this system only requires a high-speed camera or other electronic capture system capable of capturing video at hundreds of frames per second (or thousands of frames per second at smaller resolutions),

which is commercially available. The entire isolated cell sample can be analyzed without the need for any cell-specific labels and remain unaltered, allowing it to be collected off-chip for further characterization (e.g. cytological, genomic, and transcriptomic analysis).

Materials and Methods

Cancer cell isolation from patient samples

Patients with advanced cancer were recruited according to a protocol approved by the Institutional Review Board (UCLA-IRB#11-001798), from the Department of Radiation Oncology and the Department of Hematology and Oncology of the Geffen School of Medicine at UCLA. Blood samples were drawn from 12 patients, diagnosed with breast (N=4, 1 non-metastatic, 3 metastatic) and lung cancers (N=8, metastatic non-small-cell lung cancer, NSLC) seen at the clinics, as well as 4 healthy volunteers, and processed using the Vortex Chip. Team members processing blood and counting cells within samples were told that all samples (including healthy samples) were metastatic breast or lung patients to prevent any bias in operation or counting. Four additional breast samples and one lung sample were excluded due to errors in sample preparation during the fixation and staining steps following isolation. For clinical samples, cells were fixed and permeabilized as described previously, but stained with DAPI (Invitrogen), CD45-PE (BD), Pan-CK-FITC (Miltenyi Biotech.) and CK CAM5.2-FITC (BD) to target CK 7, 8, 18 and 19. To evaluate capture purity, leukocytes and CTCs were enumerated by 2 different persons, where leukocytes were identified as CD45+/DAPI+ cells while CTCs were defined as circular, CK+/DAPI+ cells, that ranged from 10 to 25 μm in diameter.

Size distribution measurements

Clinical samples processed through the Vortex chip were collected in one well of a 96-well plate and imaged after immunolabeling with DAPI, cytokeratin, and CD-45. Each sample was imaged with the Nikon setup described previously (Chapter II, Materials and Methods). The cells of the acquired image were then manually measured and classified based on their fluorescent classification.

Receiver Operating Characteristic (ROC) Analysis

Analysis was performed using GraphPad Prism 6 software. Fluorescent and all DAPI counts were uploaded for NSCLC and breast samples and analyzed using built-in ROC Curve column analysis.

High-speed, Label-free Imaging

At a 10X Nikon objective lens, 256 pixel by 376 pixel images are captured every 2 milliseconds (500 frames per second) to gain one measurement per particle/cell. This can be tuned so that images are captured every 0.2 milliseconds (5000 frames per second) at a resolution of 144 pixel by 376 pixel, enabling multiple measurements per incident cell. A Phantom v7.3 high-speed camera and Phantom Camera Control and Software (Vision Research Inc.) was used, but a camera with much lower specifications can be used. In order to set the imaging area, the field of view is moved while cells are being captured such that the outlet region is straight and takes up the entire field of view. The focal plane is manually adjusted using the cells captured in the last row of vortices as a guide. To capture the video, cells are released by deactuating the syringe pump, and the video is captured post-trigger.

IV. Cytological and Cytogenetic Analysis of Circulating Tumor Cells

To further improve the accuracy of analyzing isolated cells following isolation, the eluted cell sample can be analyzed for atypical morphologies through cytology and cytogenetics. Developing CTC isolation technologies, especially affinity- and microfilter-based approaches, are limited by their ability to release cells from their devices post-isolation[31][34]. These technologies have treated captured cells with trypsin to release them or developed new cytological staining protocols adapted for their devices. Though these methods have demonstrated successful cytological analysis, their technology prevents compatibility with highly automated and standard cytological equipment and requires cytotechnicians to learn new protocols. Alternative label-free isolation approaches that are capable of isolating cells in suspension are unable to concentrate cells into a smaller liquid volume and require other methods to fix cells onto glass slides[31]. Furthermore, the low purity isolation achieved complicates imaging and analysis, where there may still be a high background of contaminating blood components. Despite these challenges, there exists a need to adapt to standard cytological protocols for ease of use and to facilitate clinical integration.

Standard cytological analysis is performed on primary tumors or biofluids (i.e. pleural fluids, ascites) that may harbor malignant cells. The staining procedure involves a series of solution exchanges and incubation steps in different reagents and is typically performed on tumor slices, where an abundant source of cells is available. Thus, cell loss throughout this protocol, where cells are precipitated onto a microscope slide and dipped into different dyes, is negligible. However, CTCs are extremely scarce and can easily be washed away during this staining protocol. An alternative technique known as CytoSpin can be performed for less cellular samples but this process involves a solution transfer step that can be a source of loss.

Since the Vortex chip can already release cells in suspension, a system that can collect cells onto a glass slide and prevent cell loss during staining protocols will be able to easily interface with traditional cytology equipment. In order to collect cells onto a glass slide, cells

released in suspension can be collected in a confining ring placed on top of a glass slide (Figure 11). In a process similar to fabricating microfluidic devices with polydimethylsiloxane (PDMS), we designed an analogous system where this confining ring, made of PDMS, is bonded to a glass slide. By tuning several parameters of the traditional fabrication protocol (i.e. using glass slides that are less optimal for bonding) a seal between the PDMS and glass slide can be made that is strong enough to prevent collected liquid from leaking but not strong enough to prevent removal. This allows the eluted cells from the Vortex chip to be collected in suspension into this interface.

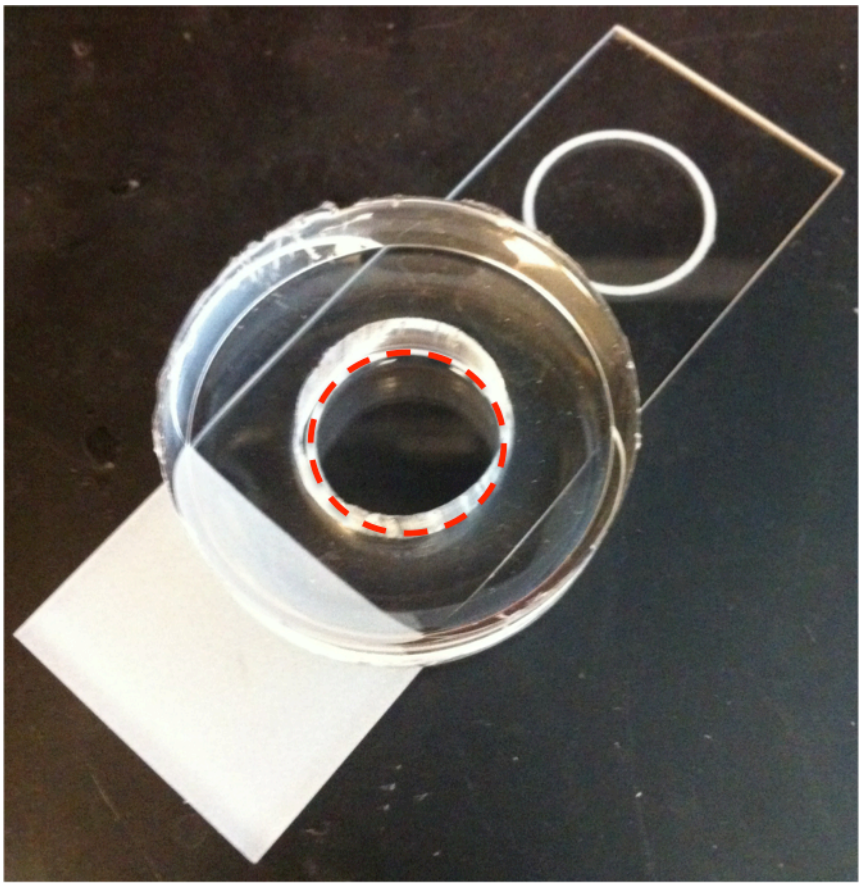

Figure 11: Cell collection system. A ring of PDMS is bonded to a glass slide that allows cells in suspension to be collected without leakage while maintaining a reversible bonding. After evaporation, the PDMS can be easily removed and the slide can be taken for cytology staining.

In order to prevent cell loss during staining, an agar/ethanol solution is introduced to the isolated cell sample. As the solution evaporates, the remaining agar forms a matrix with a monolayer of cells that allows staining dyes to perfuse while keeping cells fixed onto the slide. Once dried, the PDMS ring can be easily removed and the slide can be stained on traditional automated cytology equipment.

Using this collection method, the output of the Vortex chip is easily adapted to standard and automated cytological protocols. A conventional Papanicolau stain (Pap stain) was performed on 10 NSCLC patient samples following isolation and collection using this system (Figure 12). A team of trained cytopathologists then independently analyzed these slides and detected highly atypical cells in nine of the ten samples. Furthermore, four samples were compared to their respective primary tumor sections to demonstrate a shared site of origin (Figure 13). From a qualitative comparison, the cytopathologists noted similar and shared morphological signatures, indicating that these circulating cells may have metastasized from the primary tumor. Despite this analysis and very defined morphologies characteristic of cancer, pathologists typically reserve diagnosis until further characterization can cross-validate atypia in these findings. Patient information for each sample above is shown in Figure 14. We see a lower number of potential CTCs isolated across all samples than compared to immunofluorescence counts (Figure 7). This elevated number of cytokeratin positive cells may indicate false positive cytokeratin signals or epithelial/endothelial cell contamination during the blood draw. This provides further evidence that immune-based detection operates best when accompanied with other modes of analysis.

The detection of highly atypical cells through morphological analysis demonstrates another mode of analysis for cross-validation. With highly heterogeneous cytokeratin expression in cancer, cytological analysis enables a complementary technique to increase the accuracy of analysis and potentially identify a subpopulation of CTCs that have little to no cytokeratin expression. These cells also remain physically unaltered due to a completely label-free isolation

approach- isolated cells are not bound to any exogeneous surface proteins or immunomagnetic beads and are free of deformation in micro-pores. Cell morphologies remain preserved with this isolation technique and are almost completely free of contaminating blood cells, both of which are important for accurate analysis by cytopathologists. Furthermore, the release of cells in suspension from the Vortex chip and collection system readily enables clinical integration with existing cytology equipment, much of which is already automated. This eliminates the need to train cytotechnicians to perform new manual staining procedures directly on microfluidic isolation devices or micro-porous filters.

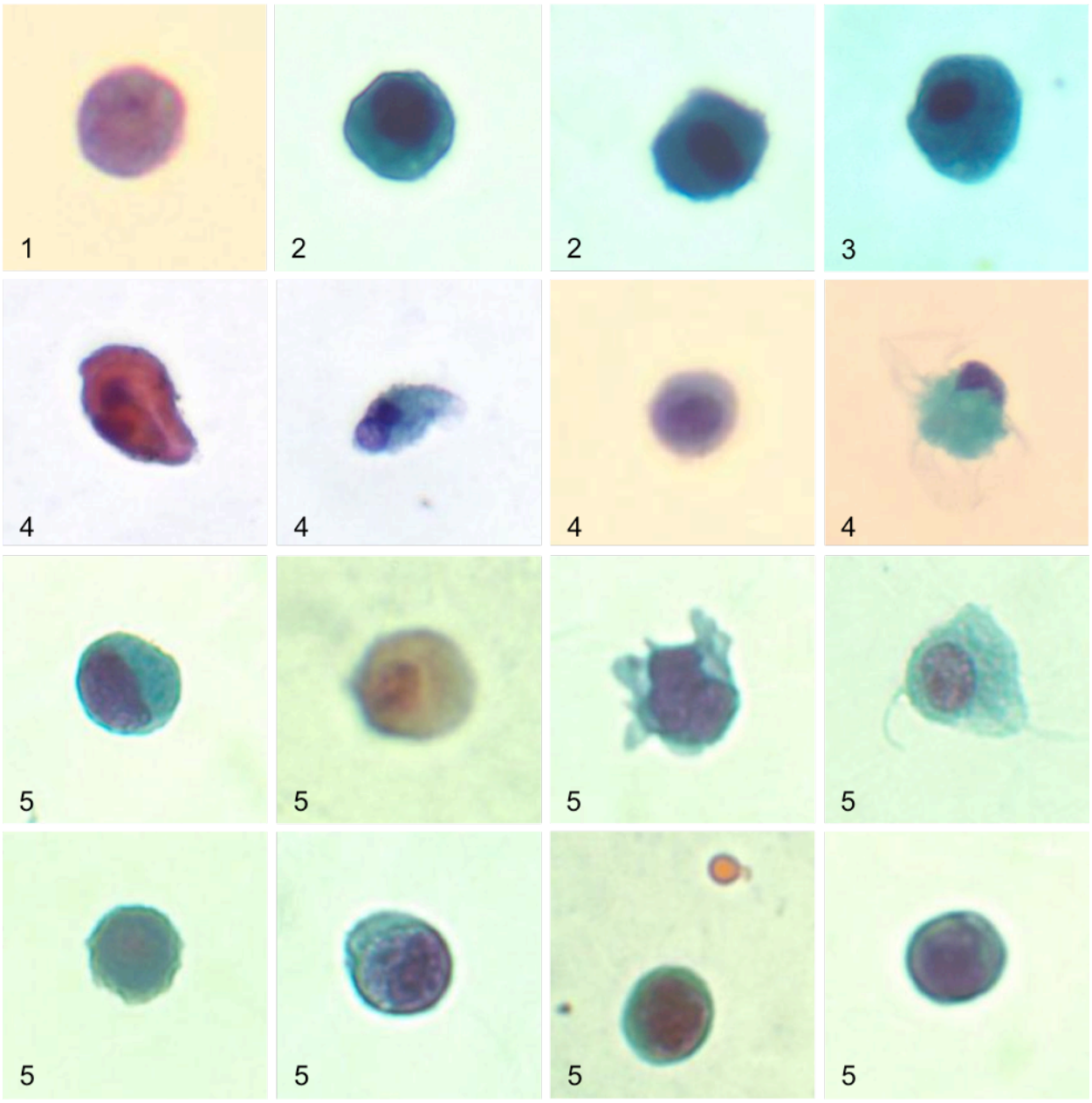

Figure 12: Highly atypical cells from NSCLC patient blood. Cells detected after isolation and conventional Papanicolaou staining with the Vortex chip. The number corresponds to the patient number.

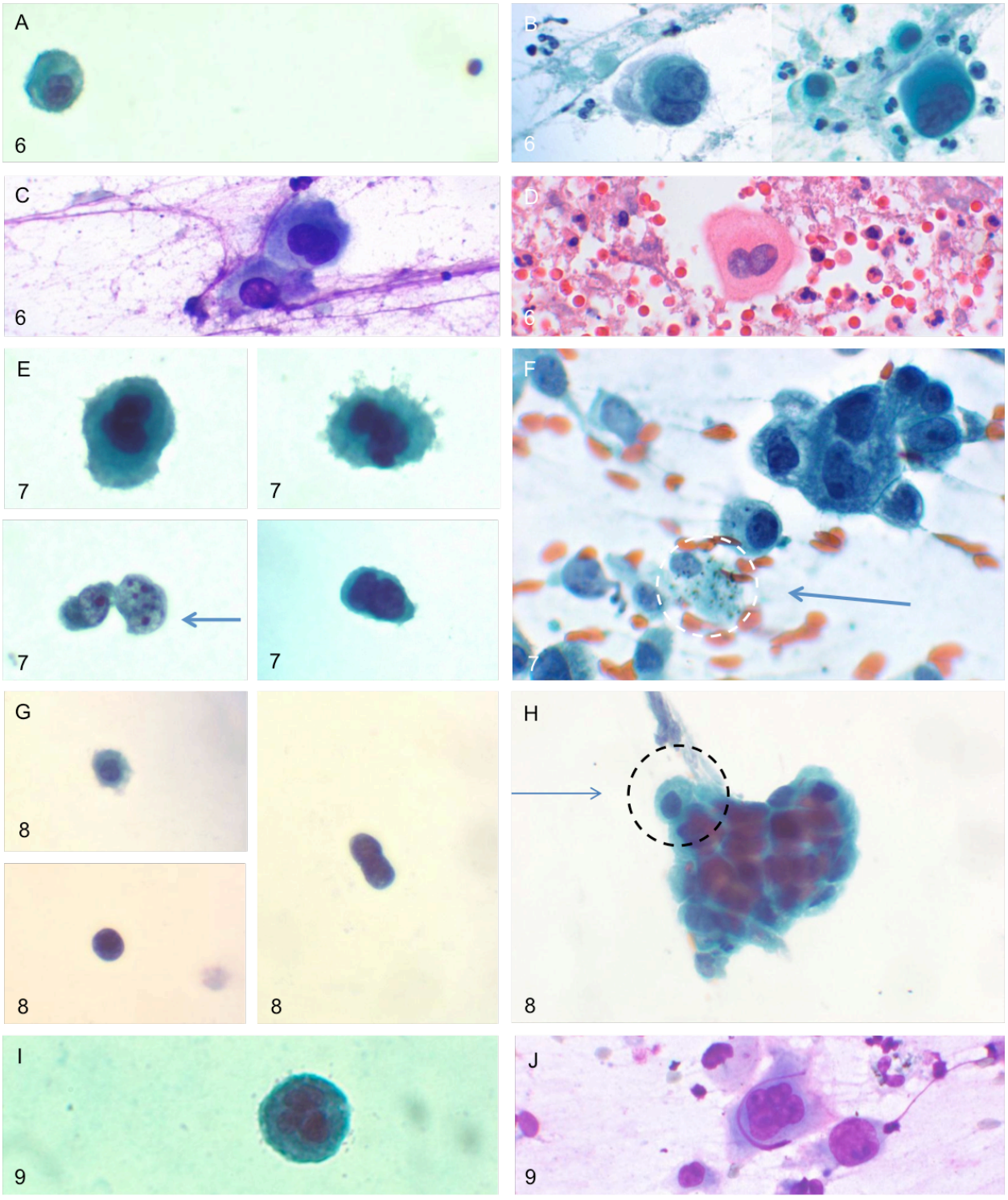

Figure 13: Cytological comparison with primary tumors. Comparison of isolated circulating cells with primary tumor samples reveals similar morphological similarities. (A-D) In sample 6, large cell size and a binucleation can be seen in (B) a conventional Papanicolaou stain and (C) May-

Grünwald-Giemsa (MGG) stain of a pleural fluid and (D) hematoxylin and eosin (H&E) stain of a cell block. (E) Isolated cells in sample 7 have a very high NC ratio and have a distinct chromatin margination pattern that is seen in (F) a Papanicolaou stain of a fine needle aspirate. (G) Sample 8 contains circulating cells and cells from (H) a core needle biopsy with irregular nuclear contours and hyperchromasia. (I) Very large cells with multinucleation are seen in sample 9 in circulation and (J) in Diff-Quik stain of tumor biopsy.

Patient #	Vol. (mL)	Atypical Cells	Atypical Cells/ mL blood	Clinical Notes
1	7.3	1	0.137	Metastatic ADN (metastases to bone, brain, and liver)
2	8	3	0.375	Metastatic ADN
3	8	1	0.125	Metastatic ADN
4	7.7	5	0.649	Metastatic ADN
5	8	6	0.137	ADN (staging not yet complete); diagnosed one month prior to processing
6	8	1	0.125	Metastatic ADN, off chemo for 12 months, stable until progression seen three months prior to processing
7	8	4	0.500	Metastatic ADN, off chemo for 20 months, NED at Stage IIIa until recent recurrence at Stage IV
8	8	3	0.375	Metastatic SCC (metastases to liver, bones, malignant pleural effusion); diagnosed one month prior to processing
9	10	1	0.100	Metastatic SCC (metsases to hip and bone); diagnosed with new lung primary three months prior to processing
10	9	0	0.000	Metastatic SCC (metsases to brain); diagnosed eight months prior to processing

Figure 14: Cytology patient information. Patient numbers correspond to Figures 12 and 13. Volume represents the volume of blood processed through the Vortex chip. ADN = adenocarcinoma, SCC = squamous cell carcinoma, NED = no evidence of disease.

Another standard analysis procedure that is performed is fluorescence *in situ* hybridization (FISH, which is used to detect specific genetic aberrations and provide a fluorescent readout. Though this is a label-based approach, detection with this method is highly

sensitive and specific. Furthermore, positive identification of a specific genetic mutation can directly guide physicians towards proper treatment. Here, we examine the anaplastic lymphoma kinase (ALK) translocation, which is apparent in 3-7% of patients with NSCLC[46]. A segment of the ALK gene locus on chromosome 2 is capable of undergoing a rearrangement to give rise to an aberrant EML4-ALK fusion protein. Thus, cells negative for the translocation will exhibit two overlapping red and green probes, giving a yellow signal. Positive cells will contain either one yellow signal and separated red and green probes or two translocations. Greater than 15% of analyzed nuclei from the primary tumor must be classified as positive for the rearrangement in order to deem the patient ALK positive and suitable for crizotinib treatment. Detecting this mutation is of high interest to physicians because a US Food and Drug Administration (FDA) - approved drug, crizotinib, can act against the fusion protein and lead to improved patient survival rates[47]. Thus, detecting the ALK translocation in cells isolated from the blood of an ALK positive patient would indicate the origin and metastatic nature of the isolated circulating cells and also demonstrate the utility of a minimally invasive ALK detection and monitoring method.

Pailler et al. demonstrated feasible isolation and detection of the ALK rearrangement in CTCs but their filter-based technique requires a custom filter adapted FISH (FA-FISH) protocol[34]. Additionally, the low purity of this approach necessitated the use of an automated imaging system and software. Isolated cells were imaged after each staining protocol (cytokeratin staining, Pap staining then FISH), which allowed the automated software to cross correlate the results of each stain to discern which of the captured cells were CTCs. This requires the integration of not only a new filter adapted FISH protocol but also the use of an automated stage and imaging software to cytogenetics laboratories.

Standard cytogenetic protocols are performed on cells on a microscope slide, as with standard cytological methods. Thus, the same collection scheme (Figure 11) can be used to collect these rare cells from the Vortex chip to be used for standard FISH protocols and limit

solution transfer steps that lead to cell loss. Since these preparation methods are much more delicate in nature, there is less chance for cell loss during staining procedures and thus, the agar/alcohol solution is not needed. Additionally, the auto-fluorescence of the agar complicates imaging and analysis.

In order to demonstrate that any pre-processing steps with the Vortex chip did not prevent FISH analysis, cultured HeLa cells (Cervical cancer) were processed through the device and collected onto a glass slide. After drying, the FISH protocol was performed and analyzed for polysomy of chromosomes 12 and 21. Indeed, we were able to show multiple copies in cells after processing, indicating that the upstream processes were not damaging the cell nuclei and preventing the ability to perform accurate FISH analysis (Figure 15).

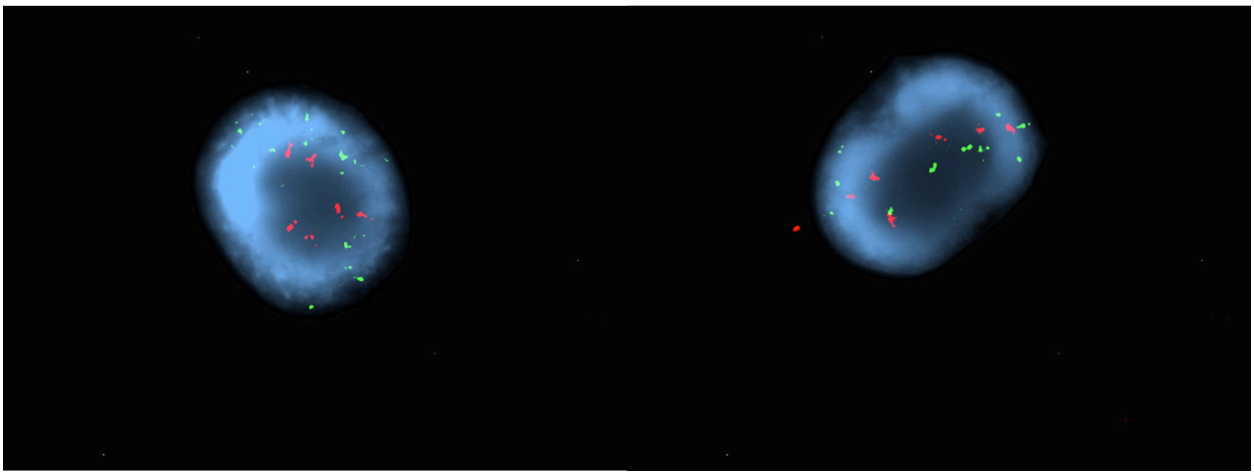

Figure 15: Vortex chip and collection procedures do not affect FISH analysis. HeLa cells successfully stained with DAPI (nucleus, blue) ETV6 (12p13, green) and AML1 (21q22, red) probes, revealing an expected polysomy.

A blinded study was performed on five samples to study possible isolation and detection of ALK positive cells in blood. The primary tumors of all patients were tested for the ALK rearrangement with the FDA-approved Vysis ALK Break Apart FISH Probe Kit, where three

patients tested positive (patients 1-3, Figure 16) and two negative (patients 4-5). Indeed, we were able to isolate and detect ALK positive cells from patients 1-3 at varying levels (patient 1:

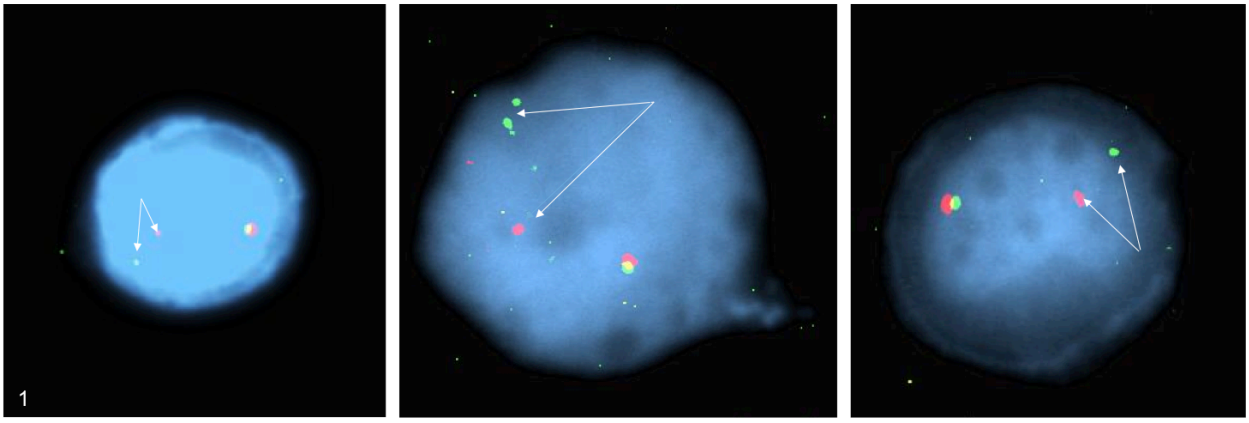

Figure 16: Successful isolation and detection of ALK positive cells from blood. Three representative ALK positive cells from patient 1 in which a clear rearrangement can be seen.

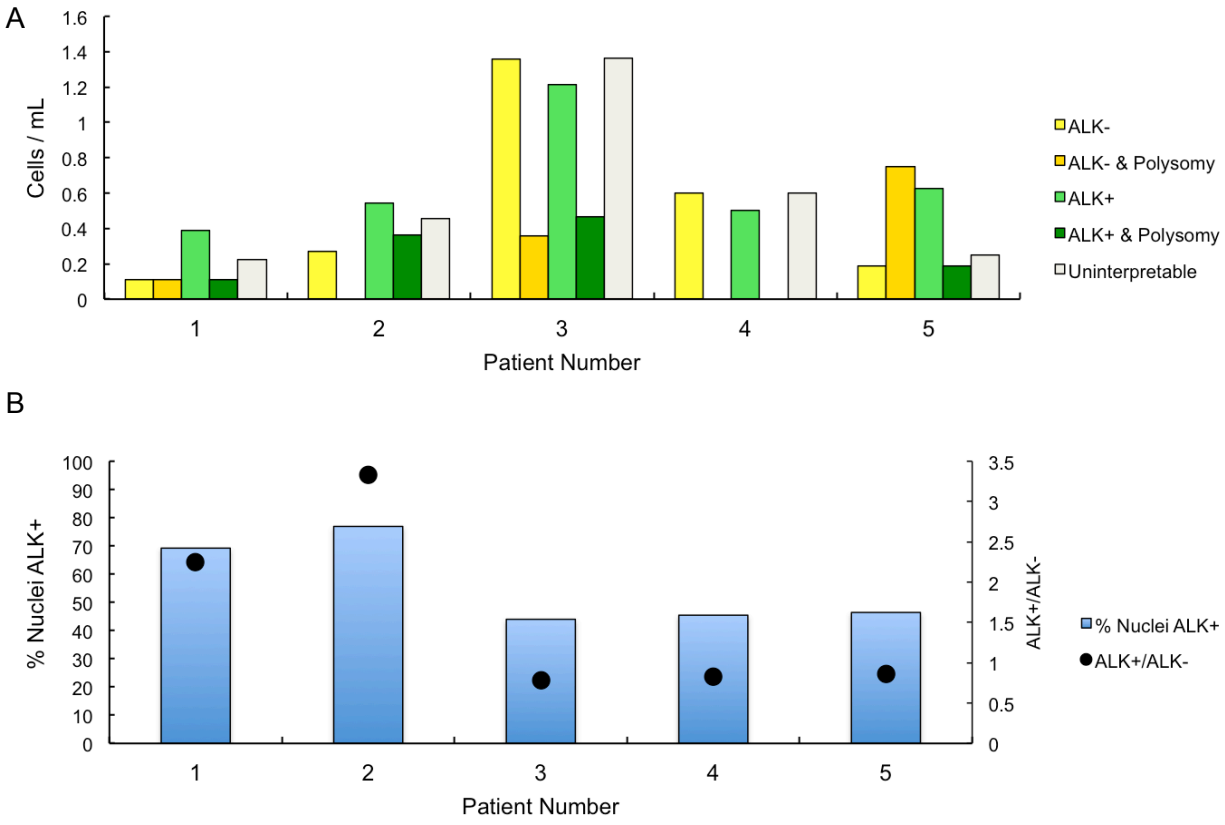

Figure 17: Detection and monitoring of the ALK translocation through CTCs. Patients 1-3 are ALK-positive, patients 4-5 are ALK-negative. (A) Enumeration and classification of isolated cells. ALK- corresponds to nuclei with two yellow signals, ALK- & Polysomy corresponds to nuclei with more than two yellow signals, ALK+ corresponds to nuclei with rearrangement, and ALK+ & Polysomy corresponds to nuclei with more than two rearrangements. Uninterpretable nuclei were classified as nuclei that had contaminating noise, where signals were extremely saturated or faint. (B) Analysis of data from (A) that shows the percentage of all nuclei analyzed that have the translocation and a ratio of ALK+ to ALK- nuclei.

0.5 ALK+ cells/mL, patient 2: 0.9 ALK+ cells/mL, patient 3: 1.7 ALK+ cells/mL, Figure 17A). The shared genetic signature demonstrates that these isolated cells are metastasizing cells with origins in the primary tumor. Interestingly, ALK positive cells were isolated and detected in patients 4-5 as well and sometimes at higher frequencies than positive patients (patient 4: 0.5 ALK+ cells/mL, patient 5: 0.8 ALK+ cells/mL).

Since the FDA-approved Break Apart Kit specifies a 15% threshold for the ALK translocation, we analyzed these isolated cells to define a new threshold to enable ALK diagnosis and monitoring from blood. From the eluted cell samples, we see a high percentage of ALK+ nuclei in patients 1 and 2 (69.2% and 76.9%, respectively) but a much lower percentage in patients 3-5 (44.0%, 45.5%, 46.4%, Figure 17B). To normalize this to background cells isolated, we also calculated an ALK+: ALK- ratio that gave a similar trend.

The high background of ALK negative cells in patient 3 complicates the establishment of a threshold for ALK detection for cells in blood. However, these cells may also be other metastasizing cells or white blood cells. Thus, looking at a metric that is independent of ALK negative cells, such as total ALK positive cells/mL blood, may be more accurate for this analysis. Although patients 1 and 2 were detected to have similar frequency of ALK positive cells as negative patients 4 and 5, this could be attributed to the treatment history of these

patients, both of whom have been on crizotinib for more than a year (Figure 18). Patient 3, however, has not, which may indicate the presence of such high numbers of ALK+ CTCs.

Patient #	Vol. (mL)	ALK-	ALK- & Polysomy	ALK+	ALK+ & Polysomy	Uninterpretable	Clinical Notes
		ALK-/mL	ALK- & Polysomy /mL	ALK+/mL	ALK+ & Polysomy /mL	Uninterpretable/mL	
1	18	2 0.111	2 0.111	7 0.389	2 0.111	4 0.222	Metastatic ADN (metastases to bilateral lung); EGFR wt, KRAS wt, ALK+; diagnosed 41 months prior to processing; on crizotinib cycle 56 at time of collection
2	11	3 0.273	0 0.000	6 0.273	4 0.273	5 0.273	Metastatic ADN (metastases to brain and spine); EGFR wt, ALK+ (91/300 nuclei); diagnosed at stage III nine years prior to processing; on crizotinib for 27 months prior to processing
3	18	9 0.500	5 0.278	7 0.389	4 0.222	15 0.833	Metastatic ADN (metastases to brain); ALK+; diagnosed four months prior to processing; currently on crizotinib
4	18	6 0.333	0 0.500	5 0.278	0 0.000	6 0.333	Metastatic adenocarcinoma (metastases to spine and brain); EGFR wt, ALK-; diagnosed at stage IV two months prior to processing
5	16	3 0.188	12 0.750	10 0.625	3 0.188	4 0.250	Metastatic ADN (metastases to bone); EGFR L858R mutation, KRAS wt, ALK-, Polysomy 2 (190/300 nuclei); diagnosed at stage IV 12 months prior to processing

Figure 18: Cytogenetics patient information. Patient numbers correspond to Figures 16 and 17. Volume represents the volume of blood processed through the Vortex chip. ADN = adenocarcinoma, EGFR = epidermal growth factor receptor, KRAS = Kirsten rat sarcoma.

Interestingly, a large population of ALK- & polysomy cells were detected in patient 5, which agreed with the polysomy of chromosome 2 apparent in the primary tumor. Detecting other genetic aberrations can increase molecular understanding and may provide clinically important information for research in developing new treatment.

We have demonstrated another supplemental analysis mode to further validate the presence of malignant cells isolated from the Vortex chip. As with cytology analysis, the collection method was easily adapted to current FISH protocols without the need for any post-

isolation processing or specialized staining protocols. Additionally, the high purity isolation achieved enables facile imaging and analysis. The presence of a high background of ALK- white blood cells would make it difficult to analyze ALK negative CTCs were that may also be metastatic. Thus, minimizing the capture of white blood cells may also allow the analysis of ALK negative CTCs, or more accurately in conjunction with other FISH probes, as a further prognostic marker. The successful detection of the ALK translocation in isolated cells in conjunction with label-free, immunological, and cytological analysis can give physicians crucial information regarding the prognosis of a patient and even the presence of a specific mutation that can be treated with a certain drug. Though this study does not define a new threshold level for ALK+ cells in blood, this can be easily be scaled up to include many more patients in a clinical trial. Furthermore, the presence of ALK positive cells in blood, even if just one cell, is clearly atypical and may be crucial prognostic information to physicians.

Materials and Methods

Cell Collection System

PDMS is poured into a 6 well plate at a cross-linker to polymer ratio of 1:10. After curing, the PDMS is removed and punched with a 17-mm biopsy punch. The resulting ring is bonded to a microscope slide using the same plasma bonding techniques described previously (Chapter II, Materials and Methods). The collection system is then filled with 800 μL of 95% ethanol such that cells collected from the Vortex chip are eluted directly into a fixative solution. For cytology preparation, 800 μL of ClearPrep (Resolution Biomedical) is placed on top. The slides are then placed in a petri dish that is shaken while evaporation on a shaker (VWR 3500 Orbital Shaker). After evaporation, the PDMS can be removed and the slide can be taken for staining.

Cytology staining

Slides are stained using a Sakura Tissue-Tek DRS2000 with a conventional Papanicolaou method. The stainer is filled with various reagents including Hematoxylin, Eosin Azure, Orange G, 70% ethanol, 95% ethanol, 100% ethanol, DI water, and xylene-substitute (Thermo Scientific). After staining, slides are then coverslipped with mounting medium and xylene.

Cytogenetic Analysis

Positively charged slides are used to make the cell collection system (Fisherbrand Superfrost Plus). The positive charge allows cells to have better adhesion to the glass slide for standard FISH staining protocol. The Vysis LSI ALK Break Apart FISH Probe Kit (Abbot) was used for the ALK study. After annealing, the slide is then analyzed on a fluorescence microscope (Axio Observer, Zeiss) with 63X and 100X oil immersion objective lenses. All images are imaged at 100X with 1.6X magnification.

V. Conclusions and Future Directions

Detecting metastatic cancer early remains essential in improving cancer patient outcome. Circulating tumor cells, which are believed to constitute the seeds of metastasis, may provide a biomarker for earlier detection and developing better metastasis drugs. However, these cells are difficult to extract from blood as they are extremely scarce and exist among a high background of contaminating blood components. Although many researchers have developed methods to isolate CTCs, their low purity isolation methods cause a dependence on label-based detection methods to improve the sensitivity of their assay. However, heterogeneous expression levels in cancer may lead these assays to miss an important subpopulation of malignant cells.

Here, we demonstrate the utility of the Vortex chip as a method to isolate circulating tumor cells and a platform technology to enable more accurate downstream analysis. The highly pure isolation achieved can enable analysis with label-free approaches as well as with standard cytology and cytogenetics. We have developed a passive and automated system to acquire label-free data from cells extracted with the Vortex chip. Additionally, we have also designed a collection system that allows the eluent to be collected and interfaced with established clinical laboratory procedures. These analysis methods in conjunction may provide more accurate information that can help guide physicians to administer more effective treatment.

With this passive system to collect label-free data from captured cells, we plan to collect cell measurements to build a database with numerous patient samples with different tumor types. This database can then be analyzed with machine learning algorithms to elucidate a biomarker, such as number of cells isolated above a certain size or with a distinct morphology, that correlates strongly with disease state. The passive data acquisition also allows direct comparison to immunofluorescence detection assays performed on the collected cell samples.

Furthermore, we plan to expand the ALK study to encompass more patients. The initial clinical study performed to demonstrate the utility of the breakapart probe was validated on 80

patients. Thus, a similar study must be done to redefine a new threshold to enable diagnosis and monitoring treatment with ALK positive cells in blood. The detection of other genetic aberrations also enables integration with a panel of different FISH probes to increase molecular understanding of unique molecular signatures that may aid in treatment development. The high specificity and sensitivity of such an assay could potentially enable a screening tool for detection of genetic aberrations from circulating cells in patients with less advanced disease.

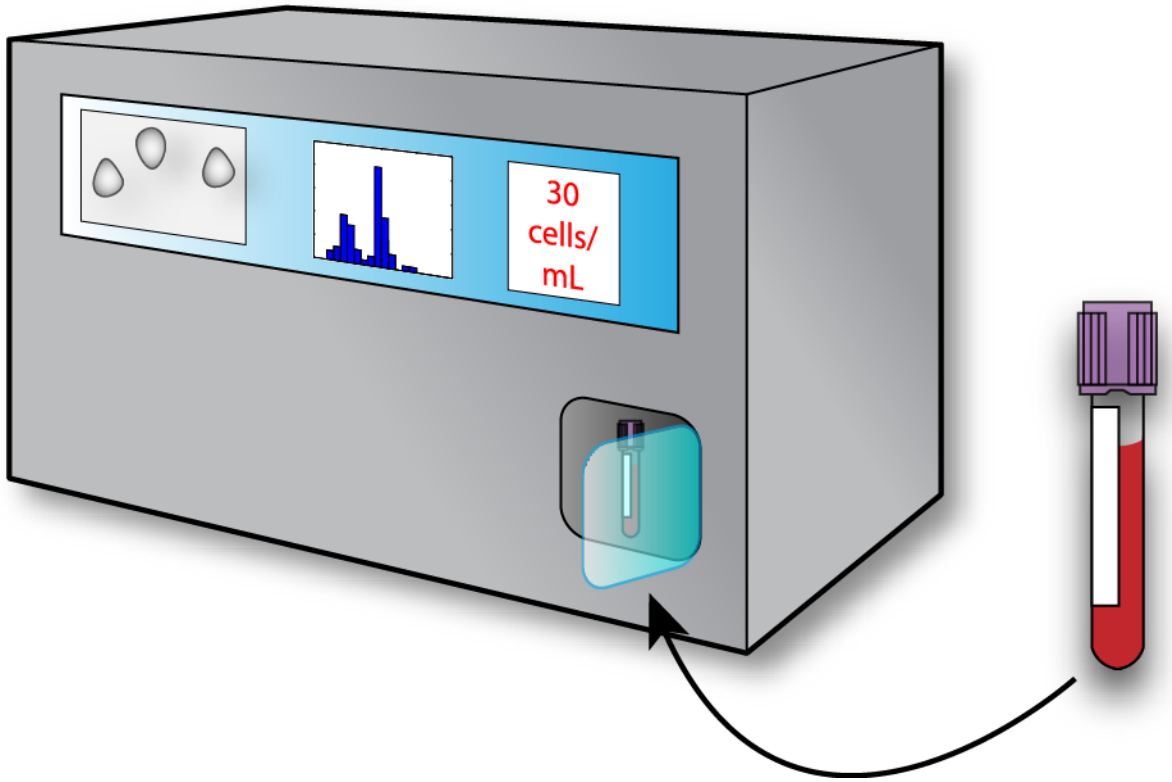

Figure 19: Clinical integration of a label-free isolation and automated cell analysis system. Full automation enables adoption into a clinical setting, where a simple input of a blood sample can output clinically important information. Cell measurements that may correlate to disease state can be quickly extracted to help improve clinical decision-making.

Lastly, the automated nature of device operation enables integration in a closed box system. This will facilitate integration, where an instrument can be utilized in a clinic and only

require a blood sample as an input (Figure 19). After processing, the system can output a quick readout with a label-free biomarker of disease state and determine if the sample is suitable for further analysis.

VI. References

[1] C. L. Chaffer and R. A. Weinberg, “A Perspective on Cancer Cell Metastasis,” *Science*, vol. 331, no. 6024, pp. 1559–1564, Mar. 2011.

[2] *Surveillance of Screening-Detected Cancers (Colon and Rectum, Breast, and Cervix) --- United States, 2004--2006*. Centers for Disease Control and Prevention, Department of Health and Human Services, 2010.

[3] E. P. Whitlock, J. S. Lin, E. Liles, T. L. Beil, and R. Fu, “Screening for Colorectal Cancer: A Targeted, Updated Systematic Review for the U.S. Preventive Services Task Force,” *Ann. Intern. Med.*, vol. 149, no. 9, pp. 638–658, Nov. 2008.

[4] H. D. Nelson, K. Tyne, A. Naik, C. Bougatsos, B. K. Chan, and L. Humphrey, “Screening for Breast Cancer: An Update for the U.S. Preventive Services Task Force,” *Ann. Intern. Med.*, vol. 151, no. 10, pp. 727–737, Nov. 2009.

[5] W. W. Moses, “Fundamental Limits of Spatial Resolution in PET,” *Nucl. Instruments Methods Phys. Res. Sect. Accel. Spectrometers Detect. Assoc. Equip.*, vol. 648 Supplement 1, pp. S236–S240, Aug. 2011.

[6] B. M. Fischer, M. W. B. Olsen, C. D. Ley, T. L. Klausen, J. Mortensen, L. Højgaard, and P. E. G. Kristjansen, “How few cancer cells can be detected by positron emission tomography? A frequent question addressed by an in vitro study,” *Eur. J. Nucl. Med. Mol. Imaging*, vol. 33, no. 6, pp. 697–702, Jun. 2006.

[7] V. Plaks, C. D. Koopman, and Z. Werb, “Circulating Tumor Cells,” *Science*, vol. 341, no. 6151, pp. 1186–1188, Sep. 2013.

[8] “Circulating tumour cells,” *Nat. Rev. Cancer*, vol. 11, no. 1, pp. 3–3, Jan. 2011.

[9] A. D. Rhim, E. T. Mirek, N. M. Aiello, and A. Maitra, “EMT and dissemination precede pancreatic tumor formation,” *Cell*, vol. 148, no. (1–2), pp. 349–361, Jan. 2012.

[10] M. Cristofanilli, G. T. Budd, M. J. Ellis, A. Stopeck, J. Matera, M. C. Miller, J. M. Reuben, G. V. Doyle, W. J. Allard, L. W. M. M. Terstappen, and D. F. Hayes, “Circulating Tumor Cells, Disease Progression, and Survival in Metastatic Breast Cancer,” *N. Engl. J. Med.*, vol. 351, no. 8, pp. 781–791, 2004.

[11] K. Pantel and C. Alix-Panabières, “Circulating tumour cells in cancer patients: challenges and perspectives,” *Trends Mol. Med.*, vol. 16, no. 9, pp. 398–406, Sep. 2010.

[12] S. Nagrath, L. V. Sequist, S. Maheswaran, D. W. Bell, D. Irimia, L. Ulkus, M. R. Smith, E. L. Kwak, S. Digumarthy, A. Muzikansky, P. Ryan, U. J. Balis, R. G. Tompkins, D. A. Haber, and M. Toner, “Isolation of rare circulating tumour cells in cancer patients by microchip technology,” *Nature*, vol. 450, no. 7173, pp. 1235–1239, Dec. 2007.

[13] C. Alix-Panabières and K. Pantel, “Circulating tumor cells: liquid biopsy of cancer,” *Clin. Chem.*, vol. 59, no. 1, pp. 110–118, Jan. 2013.

[14] S. Riethdorf, V. Müller, L. Zhang, T. Rau, S. Loibl, M. Komor, M. Roller, J. Huober, T. Fehm, I. Schrader, J. Hilfrich, F. Holms, H. Tesch, H. Eidtmann, M. Untch, G. von Minckwitz, and K. Pantel, “Detection and HER2 expression of circulating tumor cells: prospective monitoring in breast cancer patients treated in the neoadjuvant GeparQuattro trial,” *Clin. Cancer Res. Off. J. Am. Assoc. Cancer Res.*, vol. 16, no. 9, pp. 2634–2645, May 2010.

[15] P. L. Paris, Y. Kobayashi, Q. Zhao, W. Zeng, S. Sridharan, T. Fan, H. L. Adler, E. R. Yera, M. H. Zarrabi, S. Zucker, J. Simko, W.-T. Chen, and J. Rosenberg, “Functional phenotyping and genotyping of circulating tumor cells from patients with castration resistant prostate cancer,” *Cancer Lett.*, vol. 277, no. 2, pp. 164–173, May 2009.

[16] M. Pestrin, S. Bessi, F. Galardi, M. Truglia, A. Biggeri, C. Biagioni, S. Cappadona, L. Biganzoli, A. Giannini, and A. Di Leo, “Correlation of HER2 status between primary tumors and corresponding circulating tumor cells in advanced breast cancer patients,” *Breast Cancer Res. Treat.*, vol. 118, no. 3, pp. 523–530, Dec. 2009.

[17] S. Paget, “THE DISTRIBUTION OF SECONDARY GROWTHS IN CANCER OF THE BREAST.,” *The Lancet*, vol. 133, no. 3421, pp. 571–573, Mar. 1889.
[18] T. Ashworth, “A case of cancer in which cells similar to those in the tumours were seen in the blood after death,” *Aust Med J*, vol. 14, no. 3, pp. 146–149, 1869.
[19] P. Paterlini-Brechot and N. L. Benali, “Circulating tumor cells (CTC) detection: Clinical impact and future directions,” *Cancer Lett.*, vol. 253, no. 2, pp. 180–204, Aug. 2007.
[20] J. Chen, J. Li, and Y. Sun, “Microfluidic approaches for cancer cell detection, characterization, and separation,” *Lab. Chip*, vol. 12, no. 10, pp. 1753–1767, Apr. 2012.
[21] Y.-F. Sun, X.-R. Yang, J. Zhou, S.-J. Qiu, J. Fan, and Y. Xu, “Circulating tumor cells: advances in detection methods, biological issues, and clinical relevance,” *J. Cancer Res. Clin. Oncol.*, vol. 137, no. 8, pp. 1151–1173, 2011.
[22] M. C. Miller, G. V. Doyle, and L. W. M. M. Terstappen, “Significance of Circulating Tumor Cells Detected by the CellSearch System in Patients with Metastatic Breast Colorectal and Prostate Cancer,” *J. Oncol.*, vol. 2010, p. e617421, Dec. 2009.
[23] S. Riethdorf, H. Fritsche, V. Müller, T. Rau, C. Schindlbeck, B. Rack, W. Janni, C. Coith, K. Beck, and F. Jänicke, “Detection of circulating tumor cells in peripheral blood of patients with metastatic breast cancer: a validation study of the CellSearch system,” *Clin. Cancer Res.*, vol. 13, no. 3, pp. 920–928, 2007.
[24] S. L. Stott, C.-H. Hsu, D. I. Tsukrov, M. Yu, D. T. Miyamoto, B. A. Waltman, S. M. Rothenberg, A. M. Shah, M. E. Smas, G. K. Korir, F. P. Floyd, A. J. Gilman, J. B. Lord, D. Winokur, S. Springer, D. Irimia, S. Nagrath, L. V. Sequist, R. J. Lee, K. J. Isselbacher, S. Maheswaran, D. A. Haber, and M. Toner, “Isolation of circulating tumor cells using a microvortex-generating herringbone-chip,” *Proc. Natl. Acad. Sci. U. S. A.*, vol. 107, no. 43, pp. 18392–18397, Oct. 2010.
[25] B. J. Kirby, M. Jodari, M. S. Loftus, G. Gakhar, E. D. Pratt, C. Chanel-Vos, J. P. Gleghorn, S. M. Santana, H. Liu, J. P. Smith, V. N. Navarro, S. T. Tagawa, N. H. Bander, D. M. Nanus, and P. Giannakakou, “Functional Characterization of Circulating Tumor Cells with a Prostate-Cancer-Specific Microfluidic Device,” *PLoS ONE*, vol. 7, no. 4, p. e35976, Apr. 2012.
[26] A. M. Shah, M. Yu, Z. Nakamura, J. Ciciliano, M. Ulman, K. Kotz, S. L. Stott, S. Maheswaran, D. A. Haber, and M. Toner, “A Biopolymer System for Cell Recovery from Microfluidic Cell Capture Devices,” *Anal. Chem.*, vol. 84, no. 8, pp. 3682–3688, Apr. 2012.
[27] A. Marusyk, V. Almendro, and K. Polyak, “Intra-tumour heterogeneity: a looking glass for cancer?,” *Nat. Rev. Cancer*, vol. 12, no. 5, pp. 323–334, May 2012.
[28] P. T. Went, A. Lugli, S. Meier, M. Bundi, M. Mirlacher, G. Sauter, and S. Dirnhofer, “Frequent EpCam protein expression in human carcinomas,” *Hum. Pathol.*, vol. 35, no. 1, pp. 122–128, Jan. 2004.
[29] M. G. Pak, D. H. Shin, C. H. Lee, and M. K. Lee, “Significance of EpCAM and TROP2 expression in non-small cell lung cancer,” *World J. Surg. Oncol.*, vol. 10, p. 53, 2012.
[30] S. J. Tan, L. Yobas, G. Y. H. Lee, C. N. Ong, and C. T. Lim, “Microdevice for the isolation and enumeration of cancer cells from blood,” *Biomed. Microdevices*, vol. 11, no. 4, pp. 883–892, Aug. 2009.
[31] E. Ozkumur, A. M. Shah, J. C. Ciciliano, B. L. Emmink, D. T. Miyamoto, E. Brachtel, M. Yu, P. Chen, B. Morgan, J. Trautwein, A. Kimura, S. Sengupta, S. L. Stott, N. M. Karabacak, T. A. Barber, J. R. Walsh, K. Smith, P. S. Spuhler, J. P. Sullivan, R. J. Lee, D. T. Ting, X. Luo, A. T. Shaw, A. Bardia, L. V. Sequist, D. N. Louis, S. Maheswaran, R. Kapur, D. A. Haber, and M. Toner, “Inertial Focusing for Tumor Antigen–Dependent and –Independent Sorting of Rare Circulating Tumor Cells,” *Sci. Transl. Med.*, vol. 5, no. 179, pp. 179ra47–179ra47, Apr. 2013.

[32] H. W. Hou, M. E. Warkiani, B. L. Khoo, Z. R. Li, R. A. Soo, D. S.-W. Tan, W.-T. Lim, J. Han, A. A. S. Bhagat, and C. T. Lim, "Isolation and retrieval of circulating tumor cells using centrifugal forces," *Sci. Reports*, vol. 3, p. 1259, 2013.
[33] J. Streicher, B. Fabian, K. Herkner, H. Pointner, and P. M. Bayer, "Anticytokeratins are a potential source of false-positive indirect immunofluorescence assays for C-ANCA," *J. Clin. Lab. Anal.*, vol. 12, no. 1, pp. 54–59, 1998.
[34] E. Pailler, J. Adam, A. Barthélémy, M. Oulhen, N. Auger, A. Valent, I. Borget, D. Planchard, M. Taylor, F. André, J. C. Soria, P. Vielh, B. Besse, and F. Farace, "Detection of Circulating Tumor Cells Harboring a Unique ALK Rearrangement in ALK-Positive Non–Small-Cell Lung Cancer," *J. Clin. Oncol.*, vol. 31, no. 18, pp. 2273–2281, Jun. 2013.
[35] S. C. Hur, A. J. Mach, and D. Di Carlo, "High-throughput size-based rare cell enrichment using microscale vortices," *Biomicrofluidics*, vol. 5, no. 2, Jun. 2011.
[36] A. J. Mach, J. H. Kim, A. Arshi, S. C. Hur, and D. Di Carlo, "Automated cellular sample preparation using a Centrifuge-on-a-Chip," *Lab. Chip*, vol. 11, no. 17, pp. 2827–2834, Sep. 2011.
[37] E. Sollier, D. E. Go, J. Che, D. R. Gossett, S. O'Byrne, W. M. Weaver, N. Kummer, M. Rettig, J. Goldman, N. Nickols, S. McCloskey, R. P. Kulkarni, and D. D. Carlo, "Size-selective collection of circulating tumor cells using Vortex technology," *Lab. Chip*, vol. 14, no. 1, pp. 63–77, Nov. 2013.
[38] G. Segre, "Radial particle displacements in Poiseuille flow of suspensions," *Nature*, vol. 189, pp. 209–210, 1961.
[39] D. D. Carlo, "Inertial microfluidics," *Lab. Chip*, vol. 9, no. 21, pp. 3038–3046, Nov. 2009.
[40] A. A. S. Bhagat, S. S. Kuntaegowdanahalli, and I. Papautsky, "Inertial microfluidics for continuous particle filtration and extraction," *Microfluid. Nanofluidics*, vol. 7, no. 2, pp. 217–226, 2009.
[41] D. Di Carlo, J. F. Edd, K. J. Humphry, H. A. Stone, and M. Toner, "Particle segregation and dynamics in confined flows," *Phys. Rev. Lett.*, vol. 102, no. 9, p. 094503, Mar. 2009.
[42] S. C. Hur, H. T. K. Tse, and D. Di Carlo, "Sheathless inertial cell ordering for extreme throughput flow cytometry," *Lab. Chip*, vol. 10, no. 3, p. 274, 2010.
[43] H. Moffatt, "Viscous and resistive eddies near a sharp corner," *J. Fluid Mech.*, vol. 18, no. 01, pp. 1–18, 1964.
[44] D. Di Carlo, D. Irimia, R. G. Tompkins, and M. Toner, "Continuous inertial focusing, ordering, and separation of particles in microchannels," *Proc. Natl. Acad. Sci. U. S. A.*, vol. 104, no. 48, pp. 18892–18897, Nov. 2007.
[45] G. Vona, A. Sabile, M. Louha, V. Sitruk, S. Romana, K. Schütze, F. Capron, D. Franco, M. Pazzagli, M. Vekemans, B. Lacour, C. Bréchot, and P. Paterlini-Bréchot, "Isolation by size of epithelial tumor cells : a new method for the immunomorphological and molecular characterization of circulatingtumor cells," *Am. J. Pathol.*, vol. 156, no. 1, pp. 57–63, Jan. 2000.
[46] E. L. Kwak, Y.-J. Bang, D. R. Camidge, A. T. Shaw, B. Solomon, R. G. Maki, S.-H. I. Ou, B. J. Dezube, P. A. Jänne, D. B. Costa, M. Varella-Garcia, W.-H. Kim, T. J. Lynch, P. Fidias, H. Stubbs, J. A. Engelman, L. V. Sequist, W. Tan, L. Gandhi, M. Mino-Kenudson, G. C. Wei, S. M. Shreeve, M. J. Ratain, J. Settleman, J. G. Christensen, D. A. Haber, K. Wilner, R. Salgia, G. I. Shapiro, J. W. Clark, and A. J. Iafrate, "Anaplastic Lymphoma Kinase Inhibition in Non–Small-Cell Lung Cancer," *N. Engl. J. Med.*, vol. 363, no. 18, pp. 1693–1703, 2010.
[47] A. T. Shaw, B. Y. Yeap, B. J. Solomon, G. J. Riely, J. Gainor, J. A. Engelman, G. I. Shapiro, D. B. Costa, S.-H. I. Ou, M. Butaney, R. Salgia, R. G. Maki, M. Varella-Garcia, R. C. Doebele, Y.-J. Bang, K. Kulig, P. Selaru, Y. Tang, K. D. Wilner, E. L. Kwak, J. W. Clark, A. J. Iafrate, and D. R. Camidge, "Effect of crizotinib on overall survival in patients with advanced non-small-cell lung cancer harbouring ALK gene rearrangement: a retrospective analysis," *Lancet Oncol.*, vol. 12, no. 11, pp. 1004–1012, Oct. 2011.